



HAL
open science

Deformation mechanisms in a continental rift up to mantle exhumation. Field evidence from the western Betics, Spain

Gianluca Frasca, Frédéric Gueydan, Patrick Monie, Jean-Pierre Brun

► To cite this version:

Gianluca Frasca, Frédéric Gueydan, Patrick Monie, Jean-Pierre Brun. Deformation mechanisms in a continental rift up to mantle exhumation. Field evidence from the western Betics, Spain. *Marine and Petroleum Geology*, 2016, 76, pp.310-328. 10.1016/j.marpetgeo.2016.04.020 . insu-01310895

HAL Id: insu-01310895

<https://insu.hal.science/insu-01310895>

Submitted on 3 May 2016

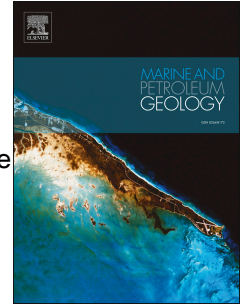
HAL is a multi-disciplinary open access archive for the deposit and dissemination of scientific research documents, whether they are published or not. The documents may come from teaching and research institutions in France or abroad, or from public or private research centers.

L'archive ouverte pluridisciplinaire **HAL**, est destinée au dépôt et à la diffusion de documents scientifiques de niveau recherche, publiés ou non, émanant des établissements d'enseignement et de recherche français ou étrangers, des laboratoires publics ou privés.

Accepted Manuscript

Deformation mechanisms in a continental rift up to mantle exhumation. Field evidence from the western Betics, Spain

Gianluca Frasca, Frédéric Gueydan, Jean-Pierre Brun, Patrick Monié



PII: S0264-8172(16)30115-5

DOI: [10.1016/j.marpetgeo.2016.04.020](https://doi.org/10.1016/j.marpetgeo.2016.04.020)

Reference: JMPG 2538

To appear in: *Marine and Petroleum Geology*

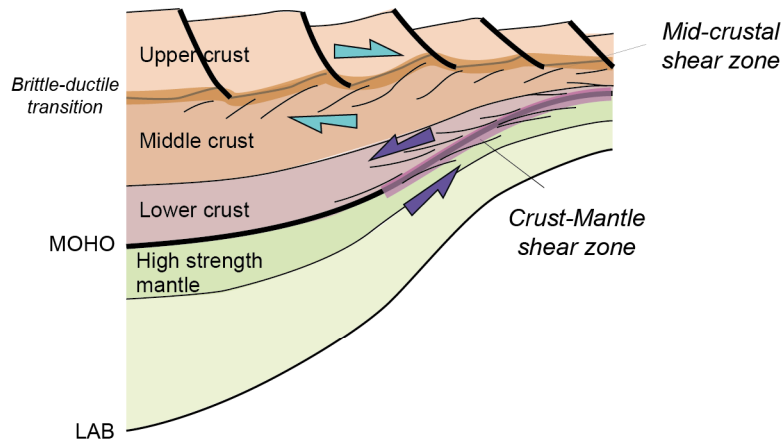
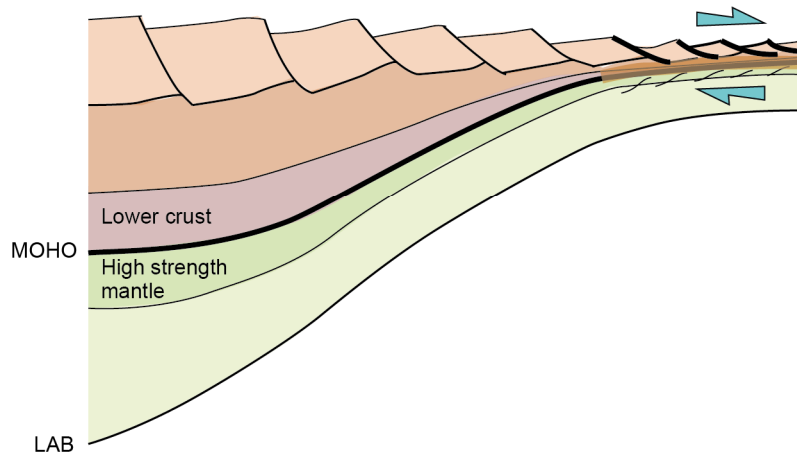
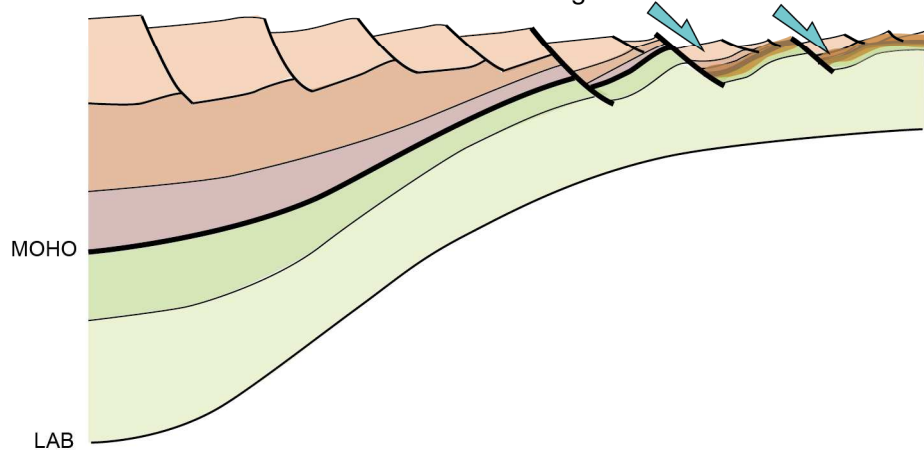
Received Date: 5 June 2015

Revised Date: 13 April 2016

Accepted Date: 20 April 2016

Please cite this article as: Frasca, G., Gueydan, F., Brun, J.-P., Monié, P., Deformation mechanisms in a continental rift up to mantle exhumation. Field evidence from the western Betics, Spain, *Marine and Petroleum Geology* (2016), doi: 10.1016/j.marpetgeo.2016.04.020.

This is a PDF file of an unedited manuscript that has been accepted for publication. As a service to our customers we are providing this early version of the manuscript. The manuscript will undergo copyediting, typesetting, and review of the resulting proof before it is published in its final form. Please note that during the production process errors may be discovered which could affect the content, and all legal disclaimers that apply to the journal pertain.

33-25 Ma; Early stages of lithosphere necking*Crust-mantle decoupling, crust heating by exhuming mantle***25-22 Ma; Advanced stages of lithosphere necking***Crust-mantle coupling, localisation (hyper-stretching), onset of cooling***22-20 Ma; Late stages of lithosphere necking***Mantle faulting & block tilting, cooling*

1 **Deformation mechanisms in a continental rift up to mantle exhumation.**

2 **Field evidence from the western Betics, Spain**

3

4

5 Gianluca Frasca^{1,2}, Frédéric Gueydan², Jean-Pierre Brun¹, Patrick Monié²

6

7 ¹*Géosciences Rennes, Université Rennes 1, UMR 6118 CNRS, Campus de Beaulieu, 35042 Rennes*
8 *Cedex, France*

9 ²*Géosciences Montpellier, Université Montpellier 2, UMR 5243 CNRS/INSU, Place E. Bataillon,*
10 *CC60, 34093 Montpellier Cedex, France*

11 *Corresponding author e-mail and telephone number: gianluca.frasca@univ-rennes1.fr; +33649326203

12

13

14

15

16 **Abstract**

17

18 The identification of the structures and deformation patterns in magma-poor continental rifted
19 margins is essential to characterize the processes of continental lithosphere necking. Brittle
20 faults, often termed mantle detachments, are believed to play an essential role in the rifting
21 processes that lead to mantle exhumation. However, ductile shear zones in the deep crust and
22 mantle are rarely identified and their mechanical role remains to be established. The western
23 Betics (Southern Spain) provides an exceptional exposure of a strongly thinned continental
24 lithosphere, formed in a supra-subduction setting during Oligocene-Lower Miocene. A full
25 section of the entire crust and the upper part of the mantle is investigated. Variations in crustal

26 thickness are used to quantify crustal stretching that may reach values larger than 2000%
27 where the ductile crust almost disappear, defining a stage of hyper-stretching. Opposite senses
28 of shear top-to-W and top-to-E are observed in two extensional shear zones located close to
29 the crust-mantle boundary and along the brittle-ductile transition in the crust, respectively. At
30 locations where the ductile crust almost disappears, concordant top-to-E-NE senses of shear
31 are observed in both upper crust and serpentinized mantle. Late high-angle normal faults with
32 ages of ca. 21 Ma or older ($^{40}\text{Ar}/^{39}\text{Ar}$ on white mica) crosscut the previously hyper-stretched
33 domain, involving both crust and mantle in tilted blocks. The western Betics exemplifies,
34 probably better than any previous field example, the changes in deformation processes that
35 accommodate the progressive necking of a continental lithosphere. Three successive steps can
36 be identified: i/ a mid-crustal shear zone and a crust-mantle shear zone, acting synchronously
37 but with opposite senses of shear, accommodate ductile crust thinning and ascent of
38 subcontinental mantle; ii/ hyper-stretching localizes in the neck, leading to an almost
39 disappearance of the ductile crust and bringing the upper crust in contact with the
40 subcontinental mantle, each of them with their already acquired opposite senses of shear; and
41 iii/ high-angle normal faulting, cutting through the Moho, with related block tilting, ends the
42 full exhumation of the mantle in the zone of localized stretching. The presence of a high
43 strength sub-Moho mantle is responsible for the change in sense of shear with depth. Whereas
44 mantle exhumation in the western Betics occurred in a backarc setting, this deformation
45 pattern controlled by a high-strength layer at the top of the lithosphere mantle makes it
46 directly comparable to most passive margins whose formation lead to mantle exhumation.
47 This unique field analogue has therefore a strong potential for the seismic interpretation of the
48 so-called “hyper-extended margins”.

49

50

51 **1/ Introduction**

52

53 During the last decades, the exhumation of subcontinental lithospheric mantle in rifted
54 margins became a commonly recognized tectonic feature. In the Iberia margin, the case-study
55 for magma-poor continental margin (Boillot et al., 1980; Boillot et al., 1987; Beslier et al.,
56 1990; Whitmarsh and Miles, 1995; Brun and Beslier, 1996), the crustal thickness decreases
57 abruptly in a short horizontal distance (75 km; Whitmarsh et al., 2001; Péron-Pinvidic and
58 Manatschal, 2009) leading to wide mantle exposures directly to the sea-floor. The sudden
59 extreme thinning of the continental crust has been well imaged through reflection seismics
60 (Péron-Pinvidic et al., 2007; Ranero and Perez-Gussinyé, 2010) and ascribed to polyphased
61 and complex activity of ductile and brittle structures (Manatschal et al., 2001; Péron-Pinvidic
62 et al., 2007).

63

64 The bulk process responsible for lithosphere thinning up to continental breakup is a
65 “necking” instability that leads to a sharp decrease in crustal thickness and to strong
66 decoupling between upper crust and mantle allowing the mantle to exhume in the rift center
67 (Brun and Beslier, 1996). The final stage of lithosphere thinning, so-called “hyperextension”,
68 is then characterized by coupled continental brittle crust and mantle. Faults penetrate into the
69 mantle and “extensional allochthons” of upper crust lie in direct contact with the mantle
70 (Beslier et al., 1993; Manatschal et al., 2001). This final stage of rifting is now well
71 documented worldwide, e.g. in the South Atlantic (Contrucci et al., 2004; Moulin et al., 2005),
72 in the Red Sea (Cochran and Karner, 2007) and in Norway (Osmundsen and Ebbing, 2008),
73 and fossil examples can be observed directly in the field in the obducted margins in the Alps
74 (Manatschal, 2004; Beltrando et al., 2012; Mohn et al., 2010, and references therein) and in
75 the Pyrenees (Clerc et al., 2012; Clerc and Lagabriele, 2014). Normal faults and detachment

76 faults shape this late stage of rift (i.e. “hyperextension”) and may obliterate the earlier
77 structures that are responsible for a large part of the lithosphere thinning. It is therefore
78 difficult to obtain a detailed resolution of the first stages of “necking” from seismic data (for a
79 detailed discussion see Reston, 2007). In the other hand, analogue and numerical models
80 reveal that large ductile shear accommodates crust-mantle decoupling and hence controls the
81 process of sub-continental mantle exhumation during lithosphere necking (Brun and Beslier,
82 1996; Gueydan et al., 2008). More generally, many aspects of the relationships between upper
83 crustal faulting and crust-mantle deformation during necking remain poorly understood. As
84 an example, fault displacements observed in seismic lines always remain rather small
85 compared to the overall crustal thinning (Reston, 2007). To reconcile such discrepancies
86 various solutions have already been considered: i) large-scale crustal detachments (Lister et
87 al., 1986; Manatschal et al., 2001; Froitzheim et al., 2006; Mohn et al., 2012), ii) upper crustal
88 brittle faulting accommodated by lower crustal flow (Brun and Beslier, 1996; Ranero and
89 Perez-Gussinyé, 2010; Gueydan and Précigout, 2014) or iii) depth-dependent mechanisms of
90 thinning at different levels in the crust (Davis and Kuszniir, 2004; Huisman and Beaumont,
91 2011).

92
93 To unravel the different stages of necking, a key issue is to characterize deformation
94 of the rifted lithosphere at different levels: subcontinental mantle, deep crust and upper crust.
95 However, sections reaching the deepest levels of a rifted lithosphere are rarely exposed in the
96 field. The large bodies of subcontinental mantle exposed in the westernmost Alboran region,
97 in the western Mediterranean, provide a unique opportunity to study the brittle and ductile
98 deformations that developed during lithosphere necking. In this region, a complete section of
99 the stretched continental crust is associated to the exhumation of the Ronda Peridotites that is,
100 with its three main massifs, the world largest outcrop of subcontinental mantle (Balanyá et al.,

101 1997; Argles et al., 1999). Major extensional shear zones located at the crust-mantle interface
102 are coeval with the subcontinental mantle exhumation (Afiri et al., 2011; Précigout et al.,
103 2013; Frets et al., 2014; Gueydan et al., 2015). The western Betics is thus a prime location to
104 observe and measure the effects of stretching at different levels of the continental lithosphere
105 (Tubía and Cuevas et al., 1986; Balanyá et al., 1997; Argles et al., 1999; Précigout et al.,
106 2013).

107

108 In the present paper, we use the outstanding field example of the western Betics to
109 study the patterns of deformation and kinematics that characterize the progressive necking of
110 a continental lithosphere. After a review of the geological and tectonic setting of the Ronda
111 peridotites, we describe i) the structural and geochronological data collected during this study,
112 ii) the major ductile shear zones located in the middle crust and at the crust-mantle transition
113 and iii) the regional gradient of thinning undergone by the crustal units. The discussion is
114 dedicated to the variations of shear sense with depth and to the processes of lithosphere
115 necking in the western Betics.

116

117

118 **2/ Geological setting**

119

120 The *Betic-Rif* belt is divided into a metamorphic Internal Zone (Alboran Domain) and
121 a non-metamorphosed External Zone (inset of Fig. 1). The Internal-External Zone Boundary
122 (IEZB) separates the Alboran Domain from an external thrust-and-fold belt (e.g. Crespo-
123 Blanc and Frizon de Lamotte, 2006; Chalouan et al., 2008). Tertiary foreland basins wrap the
124 belt to the North, West and South (Flinch, 1993; Fernández et al., 1998) (shaded in inset of
125 Fig. 1). The External Zone represents the subducting Iberian and Maghrebian margins (pale

126 grey in inset of Fig. 1) and the Alboran Domain is a portion of the upper plate of the western
127 Mediterranean subducting system (dark grey in inset of Fig. 1) (e.g. Garrido et al., 2011; Platt
128 et al., 2013). A large part of the Alboran Domain stands below sea level in the Alboran Sea
129 basin, whose development is mostly coeval with Miocene shortening in the arcuate External
130 Zone (García-Dueñas et al., 1992; Watts et al., 1993; Balanyá et al., 1997; Comas et al., 1999;
131 Platt et al., 2013).

132

133 The metamorphic tectonic units of the Alboran Domain contain in the westernmost
134 sector the Ronda Peridotites. The *exhumation* mechanism and timing of the *Ronda Peridotites*
135 have been and are still *matter of controversy*. Among the proposed mechanisms of mantle
136 rock exhumation are: i) mantle core complex (Doblas and Oyarzun, 1989), ii) crosscutting
137 detachment faults during the extensional collapse of the Betic-Rif chain (Van der Wal and
138 Vissers, 1993; Platt et al., 2003a), iii) transpressional extrusion of a mantle wedge (Tubía et
139 al., 1997; Mazzoli and Martín-Algarra, 2011; Tubía et al., 2013), and iv) inversion during slab
140 rollback of a thinned back-arc lithosphere (Garrido et al., 2011; Hidas et al., 2013; Précigout
141 et al., 2013). Ages of exhumation also strongly vary: i) Paleozoic (Kornprobst, 1976; Ruiz
142 Cruz and Sanz de Galdeano, 2014), ii) Mesozoic (Van Hinsbergen et al., 2014; Vissers et al.,
143 1995) and iii) Oligo-Miocene (Hidas et al., 2013; Précigout et al., 2013).

144

145 2.1/ The Ronda – Beni Bousera subcontinental mantle

146

147 The *Ronda Peridotites* in southern Spain consist of three main massives, called
148 Bermeja, Alpujata, Carratraca massives (Fig. 1). Several smallest mantle outcrops connect the
149 three larger massives suggesting the original continuity of a single mantle sliver (Navarro-
150 Vilá and Tubía, 1983; see Didon et al., 1973 for an alternative view). Furthermore, the Ronda

151 Peridotites in the western Betics were probably originally continuous with the Beni Bousera
152 massif (Sánchez-Gómez et al., 2002) on the Rifan side of the Gibraltar arc (inset in Fig. 1)
153 and then dismembered during the Miocene formation of the Gibraltar arc (Balanyá et al.,
154 1997; Berndt et al., 2015; Chalouan et al., 2008; Frasca et al., 2015). The peridotites display a
155 kilometer-scale petrological zoning with Grt/Sp-peridotites at the top, granular and
156 porphyroclastic Sp-peridotites in the middle and Plag-bearing peridotites at the base (Obata,
157 1980). The Ronda Peridotites sliver is separated from the Alboran continental crustal rocks by
158 *two major tectonic contacts*: i) the Ronda Peridotites Thrust at the base and ii) the Crust-
159 Mantle extensional shear zone at the top (respectively black and white colors in map and
160 cross-section of Fig. 1) (Tubía et al., 1997; Mazzoli et al., 2013; Précigout et al., 2013;
161 Johanesen and Platt, 2015).

162
163 The *Ronda Peridotites Thrust* is a “hot” thrust (Tubía et al., 1997; Esteban et al., 2008)
164 characterized by a metamorphic sole with: 1/ partial melting in the footwall metamorphic
165 rocks with ages ranging between 22 Ma and 19 Ma (Esteban et al., 2011), and 2/ high-
166 temperature minerals in the basal Mesozoic sediments deformed during Lower Miocene
167 (high-temperature: Mazzoli et al., 2013; deformed Lower Miocene Nava Breccia: Mazzoli
168 and Martín-Algarra, 2011). The Plagioclase tectonites (Fig. 1) usually mark the deformation
169 immediately above the Ronda Peridotites Thrust (Hidas et al., 2013; Précigout et al., 2013).

170
171 Conversely, the *Crust-Mantle Shear Zone* shows structural and petrological evidences
172 of an extensional nature (Tubía and Cuevas, 1986; Balanyá et al., 1997; Argles et al., 1999;
173 Sánchez-Gómez et al., 1999; Précigout et al., 2013). Garnet-spinel mylonites mark the Crust-
174 Mantle Shear Zone with a top-to-SW shearing in the Bermeja massif (Précigout et al., 2013),
175 top-to-E shearing in the Alpujata massif (Tubía and Cuevas, 1986), a variable sense of shear

176 in the Carratraca area (Tubía et al., 2004), and top-to-NW sense of shear in the Beni Bousera
177 massif (Afiri et al., 2011; Frets et al., 2014). Simultaneously, mantle rocks have recorded a
178 continuous decompression, from the garnet stability field to spinel-peridotite facies (Garrido
179 et al., 2011), related to ductile strain localization at the very top of the mantle units (Précigout
180 et al., 2007; Afiri et al., 2011; Précigout et al., 2013). Gabbros and Cr-rich pyroxenites
181 developed during mantle exhumation (Marchesi et al., 2012; Hidas et al., 2015). Nevertheless,
182 all mantle massives are dominated by spinel lherzolites in which mafic layers are common
183 (Garrido and Bodinier, 1999). The granular plagioclase-peridotites at the base are separated
184 from the overlying spinel tectonites by a “recrystallization front” that marks the asthenosphere
185 boundary (Van der Wal and Vissers, 1996; Lenoir et al., 2001; Soustelle et al., 2009) that is
186 not exposed in the Carratraca massif (Tubía et al., 2004).

187

188 *2.2/ The western Alboran crust*

189

190 The western Alboran crustal envelope of the Ronda Peridotites is mainly made of
191 Paleozoic rocks divided in two tectonic units, Alpujarride and Malaguide, which form an
192 Alpine nappe stack most probably related to subduction during the Eocene (e.g. Vergés and
193 Fernández, 2012; Platt et al., 2013). This Alpine nappe stack represents the Alboran crust, on
194 top of the Ronda peridotites, during the Oligo-Miocene evolution (Torres-Roldán, 1979;
195 Tubía et al., 1992). The intrusion of Oligocene tholeiitic dykes in both nappes indicates that
196 nappe stacking is pre-Oligocene (Esteban et al., 2013). The Alpujarrides rocks are sometimes
197 divided in granulites, migmatites, gneisses and schists (e.g. Chalouan et al., 2008). Hereafter,
198 following partly previous field observations (Balanyá et al., 1997; Argles et al., 1999), we
199 divide the entire crust –i.e. the Alpujarrides-Malaguide pair- into three lithological groups,
200 namely lower, middle and upper crust (Log of Fig. 1).

201

202 The *lower crust* is composed by pelitic granulites, characterized by cm-size garnet
203 porphyroclasts interlayered with minor marbles and rare mafic granulites and by migmatites
204 without garnet that often show disrupted and folded leucosomes. A two-step evolution of the
205 high-temperature metamorphism during the Hercynian and the Oligocene has been recently
206 discussed in Gueydan et al. (2015). The *middle crust* is, from base to top, made of i)
207 sillimanite gneisses, with some strongly stretched migmatitic leucosomes, ii) fibrolite
208 gneisses, without leucosome but still with thin needles of sillimanite, and iii) andalusite
209 gneisses, where andalusite is the only alumino-silicate represented. Quartzites, phyllites and
210 schists with rare andalusite appear close to the transition with the upper crust. The *upper crust*
211 is composed of the Malaguide rocks made of Paleozoic slates, carbonates, clastic rocks and of
212 scattered Permian terrigenous sediments and Mesozoic carbonates.

213

214 Most of the lower and middle crust rocks have amphibolite facies parageneses and
215 partial melting is concentrated in the lower crust. Note that high-pressure low-temperature
216 metamorphism reported in the area (Argles et al., 1999) is related to the pre-rift history - i.e.
217 the Tertiary nappe stacking of Malaguide and Alpujarride units (Balanyá et al., 1997) and
218 probably also the Variscan tectonic history (Ruiz Cruz and Sanz de Galdeano, 2014). The
219 lithological boundaries between lower, middle and upper crustal units roughly reflect the
220 original 650° C and 350° C isotherms related to the high-temperature metamorphism, as
221 derived by Raman spectrometry on carbonaceous material (Negro et al., 2006) (Log in Fig. 1).
222 The different units are characterized by a fairly continuous temperature increase from upper
223 to lower crustal levels (Argles et al., 1999; Negro et al., 2006). The temperature peak is
224 corroborated also by the evidence of partial melting at the very base of the crust (Platt and
225 Whitehouse, 1999) and by a total reset of low-T chronometers in almost the entire crustal

226 section, except in the shallowest levels (Monié et al., 1994; Platt et al., 2003a; Esteban et al.,
227 2004, 2013). At the onset of rifting, the continental geotherm was rather hot and characterized
228 with estimates of Moho temperatures of ~700°C (Negro et al., 2006; Gueydan et al. 2015) and
229 ~800°C (Argles et al., 1999). Estimates of initial crustal thickness vary from 50 km (Argles et
230 al., 1999) to 35-40 km (Gueydan et al. 2015). However, such differences do not affect the
231 results of the present study.

232

233 In the Alpujarrides, a *regional foliation* defined by medium-pressure/high-temperature
234 mineral assemblages showing a decrease in pressure (Balanyá et al., 1997; Argles and Platt,
235 1999; Argles et al., 1999) developed during crustal thinning becoming parallel to the Crust-
236 Mantle shear zone (Fig. 1, Précigout et al., 2013; Gueydan et al., 2015; Balanyá et al., 1997;
237 Sánchez-Gómez et al., 1999).

238

239 *2.3/ Continental rifting in a supra-subduction setting*

240

241 The parallelism of foliations in crust and mantle and their development during
242 decompression indicate that the western Alboran domain resulted from the extensional
243 exhumation of a continental lithosphere section (Argles et al., 1999). However, Hercynian,
244 Jurassic and Alpine ages (Montel et al., 2000; Sánchez-Rodríguez and Gebauer, 2000;
245 Sánchez-Navas et al., 2014) suggest that the mantle part of the section likely underwent a
246 rather complex evolution. The present paper does not aim at discussing this long and complex
247 geological evolution of the mantle but only at constraining the deformation pattern that
248 resulted from rifting and related exhumation of the lithospheric mantle. In spite of local
249 complexities, the constant crosscutting relationships reported in the previously published
250 maps (Tubía et al., 1997; Esteban et al., 2008; Mazzoli and Martín-Algarra, 2011; Précigout

251 et al. 2013; Frasca et al., 2015) show that the Lower-Miocene Ronda Peridotite Thrust
252 postdates the mantle-crust extensional shear zone. Thinning of the continental lithosphere
253 thinning therefore occurred before the Lower Miocene. Because thinning affected the Eocene
254 Malaguide-Alpujarride nappe-stack (Vissers et al., 1995), an Oligocene-early Miocene age,
255 supported by different types of data, can be argued for the rifting.

256

257 The exhumation and cooling of the mantle is dated by the garnet pyroxenites seated
258 immediately below the extensional shear zone that separates the mantle from the crust (Sm-
259 Nd age of 21.5 ± 1.8 Ma on garnet and clinopyroxene; Zindler et al., 1983) (mean Lu-Hf ages
260 of 25 ± 1 Ma or 24 ± 3 Ma on garnet; Blichert-Toft et al., 1999; Pearson and Nowell, 2004)
261 and by leucosomes stretched within the foliation in partially molten lower crust (U-Th-Pb age
262 of 21.37 ± 0.87 Ma on monazite; Gueydan et al., 2015) (U-Pb age of 22.0 ± 0.3 Ma on zircon;
263 Platt et al., 2003b). Note that mantle was exhumed from diamond crystallization conditions
264 (more than 150 km depth; Pearson et al., 1989; Davies et al., 1993) to garnet stability field
265 (70-90 km) in a previous deformation event, most probably during Jurassic Tethyan rifting
266 (Van der Wal and Vissers, 1993; Afiri et al., 2011; Garrido et al., 2011).

267

268 As summarized above, the foliation related to the *Crust-Mantle Shear Zone*, which
269 affected simultaneously the crust and the upper part of the mantle, developed during
270 decompression under high-temperature conditions. The same sense of shear is recorded in the
271 lower part of the crustal envelope (Balanyá et al., 1997; Argles et al., 1999) and in garnet-
272 spinel mylonitic zone at the top of the peridotites (Afiri et al., 2011; Balanyá et al., 1997;
273 Précigout et al., 2013; Gueydan et al., 2015). Heating of the lower crust by the exhuming
274 mantle was high enough to induce partial melting in the crustal rocks (Argles et al., 1999;
275 Platt and Whitehouse, 1999). Mantle-related magmatic activity also attests for the hot

276 conditions of continental lithosphere during rifting. The crustal emplacement of tholeiitic
277 andesites and diorite dyke swarms is likely related to mantle rising (Garrido et al., 2011), as
278 indicated by their location, mostly in the western Betics (Esteban et al., 2013), and their major
279 elements composition (Duggen et al., 2004). The dykes that are abundant in the Malaguide
280 and its Triassic sedimentary cover (Fernández-Fernández et al., 2007) emplaced in the upper
281 and middle crust during E-W stretching (see discussion in Esteban et al., 2013). The ages of
282 30.2 ± 0.9 Ma age ($^{40}\text{Ar}/^{39}\text{Ar}$ on whole rock; Turner et al., 1999) and 33.6 ± 0.6 Ma (laser
283 $^{40}\text{Ar}/^{39}\text{Ar}$ on a plagioclase from a basalt; Duggen et al., 2004) were recently confirmed by a
284 33.1 ± 1.5 Ma age (U/Pb SHRIMP on zircons; Esteban et al., 2013). Younger lower Miocene
285 ages (22-23 Ma: K/Ar age on whole rock; Torres-Roldán et al., 1986; 17.7 ± 0.6 Ma $^{40}\text{Ar}/^{39}\text{Ar}$
286 age on whole rock; Turner et al., 1999) are likely related to the thermal cooling of dykes that
287 is controlled by the country rock temperature –i.e. the latest part of the regional high-
288 temperature metamorphic history.

289
290 The westward rollback of the Alboran subducting slab is now largely accepted to have
291 shaped the arcuate Betic-Rif belt (Balanyá et al., 2007; Garrido et al., 2011; Platt et al., 2013;
292 Précigout et al., 2013; Johanesen et al., 2014) (Fig. 2). Several large-scale lines of evidence
293 support this interpretation: i) the evolution in the volcanism types (Duggen et al., 2004), ii)
294 the westward shift in the deposition of the foreland basin (Iribarren et al., 2009) and iii) recent
295 tomography imaging of the mantle (Bonnin et al., 2014; Palomeras et al., 2014). Various
296 scenarios have been proposed with significant differences in terms of timing, direction and
297 amount of displacement (Royden, 1993; Lonergan and White, 1997; Gueguen et al., 1998;
298 Wortel and Spakman, 2000; Gutscher et al., 2002; Faccenna et al., 2004; Rosenbaum and
299 Lister, 2004; Vergés and Fernández, 2012). Whatsoever these differences, an overall
300 westward trench displacement is more likely responsible for rifting in the Alboran upper plate

301 and consequent exhumation of the subcontinental mantle (Garrido et al., 2011; Hidas et al.,
302 2013; Précigout et al., 2013) (Fig. 2a). The geochemical signature of magmatic intrusions in
303 the Ronda Peridotites indicates that they were located in the subduction upper plate (Marchesi
304 et al., 2012) (Fig. 2b).

305
306 Rifting of the continental lithosphere and subsequent mantle exhumation thus occurred
307 in a supra-subduction setting during Alboran slab rollback in Oligocene-Lower Miocene. The
308 final thrust emplacement of the *Ronda peridotites* on top of the Iberian passive margin
309 corresponds to a rift inversion that occurred within the subduction upper plate in lower
310 Miocene (Hidas et al. 2013; Précigout et al., 2013) (Fig. 2c).

311

312 *2.4/ Positioning of our study*

313

314 Our study focuses on an area of the Western Alboran that displays a complete section
315 of thinned continental lithosphere. In the following, the deformation pattern is described at the
316 crust-mantle contact and in the lower, middle and upper crust. Thus, the geometry and
317 kinematics of rift-related structures are defined and the amount of crustal thinning across the
318 exhumed section of thinned continental lithosphere is estimated. Furthermore, we argue that a
319 relationship exists between the lowermost sedimentary basin and the extensional features
320 described. Finally, the implications of our results for the mechanics of lithosphere necking
321 and non-volcanic passive margin formation are discussed.

322

323 Following the estimates of Hidas et al. (2013) and Précigout et al. (2013), the amount
324 of crustal thinning in the western Alboran Domain remained moderate bringing the mantle
325 rocks at mid-crustal levels (10-15 km). Conversely, Argles et al. (1999) and Platt et al.

326 (2003a) suggest that crustal detachments brought mantle rocks to very shallow levels in the
327 Carratraca area, leaving a strongly attenuated crustal envelope (only few km thick).
328 Furthermore, the intrusion of gabbros in the Ronda Peridotites during the late stage of mantle
329 thinning confirms that the whole continental lithosphere has been affected by an extreme
330 stretching (Hidas et al., 2015).

331
332 We focused our study on the Carratraca region because it displays: i) a complete
333 lithospheric section (Soto and Gervilla, 1991; Argles et al., 1999; Tubía et al., 2004) and ii) an
334 excision of the deepest parts of the crust (Chamón Cobos et al., 1972; Cano Medina and Ruiz
335 Reig, 1990; Del Olmo Sanz, 1990). In addition, the structures related to mantle exhumation
336 are in this region rather well preserved: iii) from reworking during rift inversion (absence of
337 plagioclase tectonites related to hot thrusting) and iv) from the effects of Miocene extension
338 related to the formation of the Alboran Sea basin (Comas et al., 1992).

339

340

341 **3/ Geometry, deformation and ages of lithosphere thinning**

342

343 *3.1/ Structural map of the Carratraca massives*

344

345 The three main types of geological units of the study area are (Fig. 3a): i) mantle rocks
346 (green; dark green highlights the grt-sp mylonites), ii) the crustal envelope (purple, brown and
347 beige) and iii) the Alosaina basin that is filled with terrigenous deposits of Lower Miocene
348 age (Sanz de Galdeano et al., 1993; López-Garrido and Sanz de Galdeano, 1999; Suades and
349 Crespo-Blanc, 2013). Foliation trajectories (Fig. 3a) are drawn from 1406 measurements (see
350 also stereoplots in Fig. S1 of “supplementary material”). The N-S trending cross-section (Fig.

351 3b) is perpendicular to the main foliation trend and cuts, along 22 km from the El Chenil
352 region to the El Chorro region, the Carratraca mantle massives, the crustal envelope and the
353 Alosaina basin. The crust-mantle boundary dips northward, while the Ronda Peridotite thrust
354 is generally flat-lying. The two main high-angle normal faults of Cerro Tajo and La Robla dip
355 southward and crosscut the Ronda peridotites and its crustal envelope.

356

357 In the crustal envelope, foliations dip northward at variable angles (Fig. 3). The main
358 foliation trend is generally parallel to the condensed metamorphic isograds, from granulite to
359 greenschist facies, easing the identification of lower, middle and upper crust. Significant
360 jumps in P-T conditions occur along the Los Grenadillos fault zone (Fig. 3) that likely acted
361 as an important mid-crustal shear zone (Argles et al., 1999). Approaching the upper crust, the
362 intensity of foliation decreases, and lithological boundaries display more evidence of layer-
363 parallel brittle shear. Low-angle normal faults are common and show breccias and gouges
364 with subhorizontal striaes.

365

366 Foliation trajectories highlight the large-scale 3D geometry of the studied domain with
367 broad anticlines cored by the peridotites massives and synclines defined by upper crustal
368 levels and the Alosaina basin. The Cerro Tajo and La Robla faults are large-scale normal
369 faults (Fig. 3) that bound the peridotite massives to the south and south-east, defining the
370 three studied tilted blocks: Agua, Robla and Alosaina.

371

372 *3.2/ $^{40}\text{Ar}/^{39}\text{Ar}$ on high angle normal faults*

373

374 The Cerro Tajo and the La Robla faults put in direct contact at map-scale mantle rocks,
375 upper crustal rocks and Alosaina basin sediments (Fig. 3a), indicating large normal sense

376 offsets (up to 5 km; Fig. 3b). Both faults show a polyphased kinematic history (Soto and
377 Gervilla, 1991; Argles et al., 1999; Esteban et al., 2004). A structural and kinematic analysis
378 of the two faults has been carried out using classical brittle shear criteria (e.g. striae, mineral
379 fibers, Riedel-type shear faults or deflection of foliations) observable on 10m-scale fault
380 surfaces. The damage zones of both faults commonly show meter-scale offsets (Figs. 4d and
381 4e). Both faults display similar kinematic patterns with a principal direction of stretching top-
382 to-S or E, and a principal direction of shortening top-to-N-NW.

383
384 The La Robla fault has been interpreted as a recent normal fault (Insua-Arevalo et al.,
385 2012). Instead, the Cerro Tajo fault has been described with movements top-to-N (Argles et
386 al., 1999; Esteban et al., 2004) or top-to-S with a dextral strike-slip component (Soto and
387 Gervilla, 1991; Crespo-Blanc and Campos, 2001), during Burdigalian to Serravallian.
388 Considering the large normal offset of these faults and their obvious control on the bulk
389 structure of the area, we collected a sample of a hydrothermal tectonic breccia (Fig. 4b) along
390 the Cerro Tajo fault (Fig. 4a) in order to date displacement along these high-angle normal
391 faults. Millimetric white micas are pervasive in the very fine-grained matrix of the tectonic
392 breccia (white arrow in Fig. 4c). White micas that are not observed in the protolith of the
393 breccias define pseudomorphs after garnet (on the left in Fig. 4c) clearly indicating a neo-
394 formation of the micas during shearing in presence of fluids (see “supplementary material”
395 and Fig. S3 for further petrographic analysis). $^{40}\text{Ar}/^{39}\text{Ar}$ step heating method on the white
396 micas extracted from the matrix of the tectonic breccia give an age of 21 ± 0.3 Ma (see age
397 spectrum in Fig. 4f). Details on the method, a table summarizing the data and a complete set
398 of isotopic results are given in the “supplementary material”.

399

400 The age of these neo-formed white micas from the tectonic breccia clearly indicates
401 that at least part of the fault activity is older than what was previously reported. It is rather
402 difficult to directly attribute this age to the extensional or compressional features observed in
403 the field, since the micas were separated from fault rocks. However, the age gives a minimum
404 boundary for the activity of the major fault zone that coincides with the $^{40}\text{Ar}/^{39}\text{Ar}$ age of the
405 micas composing the regional foliation related to the extension, as described above (Monié et
406 al., 1994). On this basis and taking into account previously published data, we consider that a
407 first extensional stage, most probably at ca. 21 Ma or older, with a top-to-S sense of shear in
408 present-day coordinates (see also Soto and Gervilla, 1991) was then followed by a
409 contractional reactivation with a strong component of dextral strike-slip shear during late
410 Burdigalian (Esteban et al., 2004; Frasca et al., 2015).

411

412 *3.3/ The Alosaina basin*

413

414 The *Alosaina Basin* (here name as such for sake of simplicity) (Figs. 1 and 3) is a
415 terrigenous Aquitanian to Langhian basin that includes three main groups (Serrano et al.,
416 2007; Suades and Crespo-Blanc, 2013 and references therein). At the base, the Ciudad-
417 Granada group is Aquitanian (22-20 Ma; dark yellow in Fig. 3). In the middle, La Viñuela
418 group is Burdigalian (20-18 Ma) and at the top the “Neonumidian” olistostrome-type deposits
419 are Burdigalian - Langhian (around 18-15 Ma) (Bourgeois, 1978; Martín-Algarra, 1987). A
420 first important feature of the basin is an upward deepening trend associated to a change in
421 sedimentation-type around 20 Ma when clasts of metamorphic rocks of the Alboran Domain
422 and locally peridotites started to be deposited in the basin (Aguado et al., 1990). A second
423 important character of the basin is the important amount of olistostromic deposits that have

424 been associated to thrusting in previous studies (e.g. Suades and Crespo-Blanc, 2013; Frasca
425 et al., 2015).

426

427 Both high-angle normal faults of Cerro Tajo and La Robla (Fig. 3) are likely
428 contemporaneous to sediment deposition in the Alosaina basin because, first, they display
429 dip-parallel offsets up to 5 Km and, second, the distribution of sediments is strongly linked to
430 the location of faults. The base of the transgressive cover of the Alboran Domain (dark yellow
431 in Fig. 3a) crops out completely only near Alosaina (Bourgeois et al., 1972a, 1972b) while
432 several smaller outcrops are scattered along the unconformity with the Alboran metamorphic
433 rocks (Peyre, 1974; Sanz de Galdeano et al., 1993; Serrano et al., 2007; Alcalá et al., 2014).
434 The base of the transgressive units is lower Aquitanian, similar to the activity of the La Robla
435 fault inferred from $^{40}\text{Ar}/^{39}\text{Ar}$ dating of fault gouges (Fig. 4). These coeval onsets of
436 sedimentation in the Alosaina Basin and high-angle normal faulting in La Robla and Cerro
437 Tajo provide an important constraint for the tectonic calendar of the area.

438

439

440 **4/ Strain and kinematics in crust and mantle**

441

442 A regional foliation coeval with medium-pressure/high-temperature metamorphism
443 developed during continental rifting and related crustal thinning whose mean direction is
444 almost parallel to the condensed metamorphic isograds in both ductile crust and mantle. Two
445 types of shear indicators are observed: ductile in mantle and lower/middle crust and brittle-
446 ductile in middle/upper crust. Figure 5 shows outcrop photographs of the different types of
447 shear criteria used throughout the entire thinned section of the continental lithosphere. In
448 Figure 6, arrows represent the mean senses of ductile shear in the lower crust and mantle

449 (violet), and in the middle crust (dark blue). Two opposite senses of ductile shear, top-to-E
450 and top-to-W, are observed that will be discussed in detail below. Brittle/ductile shear (light
451 blue arrows) that are observed in the upper crust and top middle crust can be related either to
452 rifting/thinning or to local later reactivation. The criteria adopted for data selection are also
453 discussed below.

454

455 *4.1/ Kinematics of ductile deformation*

456

457 *a) In the Crust-Mantle shear zone.* In the garnet-mylonitic peridotites of the Agua and
458 Robla blocks, C'-type shear bands often associated with strongly stretched pyroxenite layers
459 give a sense of shear dominantly top-to-W (Fig. 5b and Fig. 6). Stretching lineations are
460 mainly defined by stretched orthopyroxene crystals. Pyroxenites layers that are parallel to the
461 crust-mantle boundary (Fig. 6) are deflected in the vicinity of the Cerro Tajo fault and close to
462 El Chenil, defining a slight arcuate trend. This is responsible for the dispersion of foliation
463 poles in the stereoplots (Fig. S1). In the lower crust, the main foliation is defined by biotite
464 and sillimanite and locally by strongly stretched leucosome lenses. C'-type shear bands with
465 melt injections are abundant. Sigmoidal melt pressure shadows around garnet porphyroclasts
466 and deflection of leucosomes against C'-type shear bands indicate a sense of shear
467 dominantly top-to-W (Fig. 5c). Stretching lineations that are commonly defined by quartz
468 rods and elongated K-feldspar in granulites and migmatites are subhorizontal and trend
469 mainly E-W, almost parallel to lineations in the garnet-mylonitic peridotites. In summary, in
470 the Agua and Robla blocks, the crust-mantle boundary displays a top-to-W sense of shear at
471 the base of the crust and at the top of the mantle (Fig. 6). Few top-to-E senses of shear are
472 observed but only in scattered and discontinuous brittle/ductile low-angle shear zones (Fig. 6).

473

474 *b) In the middle crust, two senses of ductile shear are observed: top-to-W in the lower*
475 *part of the middle crust and top-to-NE in the upper part of the middle crust. ENE to NE-*
476 *trending stretching lineations are defined by sillimanite needles in the upper part of the middle*
477 *crust and by still few E-W trending quartz-sillimanite rods in the lower part. Sheath folds are*
478 *common (Fig. 5f) that could partly explain the scattering in the lineation trend observed. They*
479 *indicate high to extremely high values of the principal direction of stretching ($\lambda_1 > 7.0$; i.e.*
480 *stretching >600%) in the middle crust rocks. Deflection of foliations along C'-type shear*
481 *bands, asymmetric boudinage of competent layers and sigma or delta tails around*
482 *porphyroclasts indicate a top-to-NE sense of shear (Fig. 5e) and, less frequently, a top-to-W*
483 *or SW sense of shear in the lower part of the middle crust (Fig. 5d). No superposition of the*
484 *top-to-W and top-to-NE senses of shear has been identified leading Argles et al. (1999) to*
485 *propose that deformation was co-axial. These two opposite senses of shear, their respective*
486 *location in the lower and upper parts of the middle crust and the absence of crosscutting*
487 *relationships suggest their coeval development. Moreover, the top-to-W sense of shear in the*
488 *lower part of the middle crust is in continuity with a similar sense of shear in the lower crust*
489 *and mantle. In the other hand, the top-to-NE sense of shear in the upper part of the middle*
490 *crust is in continuity with the sense of shear at the transition between brittle and ductile crust*
491 *(Fig. 6).*

492

493 *4.2/ Kinematics of brittle/ductile deformation at whole crustal scale*

494

495 In the transition between middle and upper crust, shear criteria combine mixed ductile
496 and brittle features. Asymmetric *boudinage* and C'-type shear bands in andalusite-bearing
497 quartz veins always show a top-to-E or NE sense of brittle/ductile shearing (Fig. 6g). The
498 same features are observed in both Agua and La Robla blocks and this geographic distribution

499 indicate that the observed senses of shear are related to a single deformation event and not to
500 late local reactivations. Moreover, top-to-NE sense of shear in these ductile-brittle shear
501 indicators is related to veins that contain metamorphic minerals (Fig. 6g), indicating that the
502 development of C'-type shear bands and the overall crustal thinning are related to the regional
503 high-temperature event responsible for the main foliation.

504

505 In the upper crust, the metamorphic grade becomes very low and the absence of
506 metamorphic mineral renders almost impossible the separation of shear sense indicators
507 related to crustal thinning from those resulting from late reactivation. Widespread low-angle
508 normal faults are interpreted as associated either to crustal thinning during lower Miocene
509 (Argles et al., 1999) or to middle Miocene extensional reactivation of the Alboran domain
510 during the formation of the Alboran basin (García-Dueñas et al., 1992).

511

512 Top-to-E-NE brittle-ductile shear indicators are also observed throughout the entire
513 crustal section (light blue arrows, Fig. 6) and suggest that a late top-to-E sense of brittle shear
514 affected the entire thinned continental crust with reactivation of the previous lithological
515 boundaries (see also Argles et al., 1999).

516

517 *4.3/ A gradient of ductile crust thinning: hyper-stretching?*

518

519 Important variations in crustal thickness can be inferred from the geological map and
520 cross-sections (Fig. 3). The Cerro Tajo and La Robla high-angle normal faults divide the
521 thinned continental lithosphere in three tectonic blocks (Agua, Robla and Alozaina; Fig. 6) in
522 which crustal thickness strongly differ. Map-scale crosscutting relationships indicate that
523 variations in crustal thickness, especially in the ductile crust, were acquired before high-angle

524 normal faulting, during the Oligocene-Lower Miocene rifting. These map-scale relationships
525 also exclude that variations in crustal thickness could be attributed to later tectonic events and
526 in particular to thrusting.

527
528 The variations in crustal thickness can be partly related to erosion, but only in the
529 upper crust. A strong thickness decrease is observed in the lower crust between La Agua and
530 La Robla blocks where thickness values are 560 m and 370 m, respectively). In the Alozaina
531 block the lower crust is entirely absent and the middle crust preserved only in scattered lenses
532 of few tens meters thick and locally found in direct contact with the serpentized mantle. The
533 middle crust shows a comparable thickness variation, from 1510 m to 950 m in average from
534 the Agua to La Robla blocks. The total thickness variation of the ductile crust, from 1970 m
535 to 70 m from Agua to Alozaina blocks, corresponds to a layer-perpendicular finite strain
536 $\lambda_v=0.04$ (i.e. 96% shortening). In plane strain, this would imply a layer-parallel finite strain
537 $\lambda_h=25.0$ (i.e. a bulk stretching amount of 2400%), what can be called “hyper-stretching”. Such
538 amount of thinning-stretching is entirely related to ductile strain and cannot be simply related
539 to high-angle normal faulting. The strong gradient of layer-perpendicular shortening observed
540 cannot result only from simple shear and is necessarily a combination of layer-parallel shear
541 and layer-perpendicular shortening (i.e. combination of pure shear and simple shear).

542
543 *4.4/ Kinematics of brittle/ductile deformation in the hyper-stretched continental lithosphere*

544
545 To NE of El Chenil in the Alozaina block, where the crustal section reaches its
546 minimum thickness, a low-angle normal fault (LANF) with top to the E-NE sense of shear
547 (Fig. 6) juxtaposes the upper crustal rocks (Malaguide schists at the top) and serpentized
548 mantle rocks (Fig. 8a; for detailed map and measurements see Fig. S2). Lower and middle

549 crustal rocks are strongly stretched and reduced to meter-scale lenses (Fig. 7). In addition,
550 mylonitic peridotites are not preserved and upper crustal rocks are in direct contact with the
551 spinel-tectonites through the LANF.

552
553 The fault zone whose thickness changes along strike from around 10 to 30 m,
554 maintains a characteristic structural zoning (Figs. 8a and 8b). The LANF footwall is marked
555 by a serpentinite zone of 5 to 30 meters thick with a variable degree of brecciation and several
556 outcrops of ophicalcites (Fig. 8c), suggesting the presence of hydrothermal fluids during the
557 LANF activity. In the hanging-wall, the overlying crustal rocks (Fig. 8d) are more pervasively
558 deformed and, in the core, characterized by a gouge with clasts of quartz-veins and gneisses
559 and locally blocks of ophicalcites. In the upper crust close to the fault zone, C'-type shear
560 bands indicate a top-to-E-NE sense of shear (Fig. 8e and stereoplots in Fig. S2), as in the
561 middle and upper crust described in sub-section 4.2.

562
563 The LANF is cut during the Aquitanian by the high-angle normal fault of La Robla
564 (Figs. 5, 8a and 8b), supporting a rift-related origin. Deposition of breccias and sandstones is
565 locally controlled by C'-type faults in the LANF hanging-wall (Figs. 8a and 8b). The
566 sedimentary rocks deposited at the base of the Alosaina Basin (Ciudad Granada formation,
567 Aquitanian in age) are breccias made of 1-10 cm-large angular clasts, in a sandy yellowish to
568 brownish matrix (Fig. 8f) grading upward into quartz-rich sandstones.

569
570 In summary, stretching reached its maximum value in the Alosaina block, leading to
571 the complete omission of the ductile crust. The upper crustal rocks were carried on top of the
572 serpentinitized mantle through a LANF with a top-to-E-NE sense of shear, like in the upper
573 crust but opposite to the lower crust/upper mantle.

574

575

576 **5/ Discussion**

577

578 *5.1/ Change in the sense of shear with depth*

579

580 The ductile deformation that is responsible for the development of foliation and
581 stretching lineations at regional scale is associated to a medium-pressure/high-temperature
582 metamorphism characterized by andalusite and sillimanite in the middle crust and reaching
583 partial melting in the lowermost crust in lower Aquitanian. This extensional deformation i)
584 lead to extreme ductile crust thinning as a result of so-called hyper-stretching in an EW
585 direction and ii) is characterized by a change in the sense of shear with depth, top-to-W in the
586 mantle, lower crust and lower part of the middle crust and top-to-NE in the upper part of the
587 middle crust and in the upper crust.

588

589 Top-to-E-NE brittle-ductile shear affected the entire thinned crustal section. The
590 superposition of brittle-ductile deformation on ductile fabrics indicates that the originally
591 ductile crust cooled during thinning and became part of the brittle crust during the extensional
592 process. Consistently, in the hyper-stretched portion of the continental lithosphere, where the
593 ductile crust thickness reaches its lowest value (less than few meters), a concordant top to NE
594 shearing is observed in both strongly thinned crust and serpentized mantle.

595

596 The above conclusions can be summarized graphically with their rheological
597 implications. At the onset of extension (Fig. 9a), the vertical profile of displacement is bell-
598 shaped defining: i) a top-to-E sense of shear in the upper crust and top middle crust and ii) a

599 top-to-W sense of shear in the lower crust and the sub-continental mantle. In rheological
600 terms, this change in shear sense with depth should be controlled by two strength peaks i) the
601 brittle-ductile transition in the crust and ii) a high strength layer in the sub-Moho mantle that
602 are separated by a weak decoupling layer (i.e. the ductile crust). Upper crust and mantle are
603 thus mechanically decoupled and their respective deformation is accommodated by
604 horizontal flow in the ductile crust. Two main shear zones, the “midcrustal shear zone” and
605 the “crust-mantle shear zone” control the horizontal displacement with opposite sense of shear.
606 After a significant amount of extension and thinning (Fig. 9b) the two shear zones
607 progressively merge in a single one and the upper crust and mantle becomes mechanically
608 coupled, as exemplified by the same top to NE shearing in both crust and mantle in the hyper-
609 stretched portion of the lithosphere.

610

611 *5.2/ Some remarks about late high-angle normal faulting*

612

613 The Cerro Tajo and La Robla faults (Fig. 3) are primarily normal faults which still
614 display large dip-parallel offsets, up to 5 Km. During thrusting in late Burdigalian, these
615 faults have undergone minor contractional reactivation with a component of dextral shear
616 (Soto and Gervilla, 1991; Frasca et al., 2015) that did not significantly affected their large
617 normal offset. The two faults that cut through the crust and mantle controlled block tilting in
618 the Sierra de Agua and Sierra de la Robla. Whereas their prolongation in the Alosaina basin
619 cannot be precisely mapped, few outcrops inside the basin indicate that the sediments are
620 tilted in their hanging-wall (Fig. S2). The Ciudad-Granada group (Serrano et al., 2007) is the
621 first sedimentary formation deposited in the basin (middle and late Aquitanian, 22-20 Ma). It
622 is worth noticing that the $^{40}\text{Ar}/^{39}\text{Ar}$ age that we obtained for the La Robla fault gouge is also
623 Aquitanian - 21 ± 0.3 Ma - i.e. synchronous with the early sediment deposition in the

624 Alosaina basin. The sediments are distributed in areas where the ductile crust is missing and
625 their deposition is locally controlled by top-to-ENE C'-type shear bands at the base of the
626 upper crust. The above observations and data indicate that the base of the Alosaina basin is a
627 syn-rift deposit. The Alosaina and Malaga outcrops of the Ciudad Granada group were
628 deposited at depths of less than 200 m, in a shelf environment (Serrano et al., 2007). The
629 shallow environment of the deposition is especially interesting because syn-rift sediments are
630 rarely drilled in modern passive margins (Wilson et al., 2001; Péron-Pinvidic et al., 2007).

631
632 The two faults trend at small angle to the direction of the stretching lineations in the
633 Agua and La Robla blocks. Consequently, these normal faults cannot have developed in the
634 kinematic continuity of the ductile deformation recorded in the tilted blocks. In fact, available
635 paleomagnetic data show that the studied area has undergone dextral rotations up to 60°
636 (Feinberg et al., 1996; Villasante-Marcos et al., 2003) in relation with the formation of the
637 Gibraltar arc during slab rollback (Fig.2). Consequently, the rift that lead to hyper-stretching
638 and mantle exhumation has undergone large rotations during the late stages of its
639 development and during later inversion/thrusting (Platt et al., 1995; Frasca et al., 2015).
640 Whereas it is beyond the scope of the present paper to elaborate on these large-scale tectonic
641 aspects, it is especially interesting to note that these high-angle normal faults, whose
642 development is rather late in the rift history, cut through a brittle mantle layer of more than 5
643 km thick. This demonstrates that the extreme thinning of the continental crust in the area had
644 already permitted a fast cooling of the underlying mantle.

645

646 *5.3/ Process of lithosphere necking in the western Betics*

647

648 The geological observations and the measurements carried out in the Carratraca massif
649 of the Ronda peridotites and its crustal envelope bring new light on the process of lithosphere
650 necking. Whereas the evolution of necking is progressive, it is summarized for convenience in
651 three snapshots, called early, advanced and late stages (Fig. 10).

652
653 *The early stages of necking* (Fig. 10a), which are dated between 33 and 25 Ma by the
654 intrusion of the Malaga tholeiites (Turner et al., 1999; Esteban et al., 2013), are characterized
655 by the existence of a high strength subcontinental mantle. A common sense of shear top-to-W
656 in lower crust and uppermost mantle is opposite to the sense of shear top-to-E-NE observed in
657 the middle crust (Fig. 9a). This inversion in the sense of shear with depth strongly constrains
658 the mechanical behavior of the rifted lithosphere. It shows that the ductile middle and lower
659 crust played the role of a decoupling layer (i.e. *décollement*) between the brittle upper crust
660 and the high strength subcontinental mantle. In rheological terms, it indicates that the mantle
661 strength was higher than the strength of the overlying ductile crust and underlying deeper
662 lithospheric mantle. In addition, strain weakening processes lead to strain localization both at
663 the brittle-ductile transition in the crust and in the uppermost part of the subcontinental mantle
664 (Fig 9a; see discussion in Gueydan et al. 2014). The formation of these two shear zones
665 provides a simple explanation for the observed inversion of shear sense at the boundary
666 between middle and lower crust (Fig 9a and 10a). Analogue and numerical models show that
667 lithosphere necking is accommodated by intense strain localization in the subcontinental
668 mantle (Gueydan and Précigout, 2014) and crust-mantle decoupling (crustal *décollement*)
669 (Brun and Beslier, 1996; Nagel and Buck, 2004; Gueydan et al., 2008). Moreover, modelling
670 also exemplifies that the necking process corresponds, at lithosphere scale, to a pure shear-
671 type deformation accommodated by conjugate shear zones with opposite senses of shear,
672 respectively at the base of the brittle crust and in the subcontinental mantle (Brun and Beslier,

673 1996; Gueydan et al., 2008). The strong mylonitization and thinning of the high-strength
674 mantle (Précigout et al., 2007) allows the deeper and weaker mantle to come into contact with
675 the crust, hence implying a strong heating of the lower crustal levels (Gueydan et al., 2015).
676 This is in agreement with partial melting observed in the lower part of the crust (Platt and
677 Whitehouse, 1999; Whitehouse and Platt, 2003). Such a high geotherm (Negro et al., 2006) is
678 likely related to the supra-subduction setting of rifting in the western Alboran.

679
680 *The advanced stages of necking* (Fig. 10b), which are dated between 25 and 22 Ma by
681 crystallization and cooling ages within the high-temperature foliation (Esteban et al. 2013; see
682 data compilation in section 2), are characterized by a strong thinning of the ductile crust
683 observed from the Agua to Alozaina blocks. The extremely large gradient of stretching
684 (2400%) can be qualified of “hyper-stretching”. The drastic decrease of the crustal thickness
685 triggers cooling of the attenuated crust and upper part of the lithospheric mantle.
686 Consequently, the initial strength profile with two peaks (Fig. 9a) becomes single peak in the
687 localized zone of stretching (Fig. 9b). In other words, the crust and mantle becomes
688 mechanically coupled and the two major shear zones (i.e. mid-crustal and crust-mantle shear
689 zones) merge into a single, with top to NE shearing between upper crust and serpentinized
690 mantle. Four-layers analogue models of lithosphere extension have consistently shown that
691 the boudinage of the high strength mantle was able to bring into contact the upper part of the
692 crust and the ductile lithospheric mantle with their already acquired opposite senses of shear
693 (Brun and Beslier, 1996).

694
695 *The late stages of necking* (Fig. 10c), which is dated between 22 and 20 Ma (our
696 $^{40}\text{Ar}/^{39}\text{Ar}$ minimum age on the Cerro Tajo fault and Alozaina basin), are characterized by the
697 development of steeply dipping normal faults and related block tilting within this domain of

698 localized stretching. Cooling thus occurs rapidly in the thinned crust and the underlying
699 mantle, and induces a downward migration of the brittle-ductile transition in the lithospheric
700 mantle. In the western Betics, this event of late brittle deformation is indeed superposed to
701 previous ductile fabrics and is characterized by the formation of tilted blocks of Agua, La
702 Robla and Alozaina, whose formation has been interrupted by thrusting and rift inversion
703 around 20 Ma (Frasca et al., 2015). The syn-rift deposits are coeval with this late stage and
704 mark the onset of subsidence and cooling of the stretched portion of the lithosphere.

705
706 Whereas mantle exhumation in the western Betics occurred in a backarc setting, the
707 observed deformation pattern is strongly controlled by the presence of a high-strength layer at
708 the top of the lithosphere mantle. This makes it directly comparable to most passive margin
709 formation that have lead to mantle exhumation and therefore it provides a useful field
710 analogue for the seismic interpretation of the so-called “hyper-extended margins”.

711

712 *5.4/ Field evidence versus models*

713

714 In summary, the western Betics, probably better than any previous field study,
715 exemplifies the changes in deformation processes that accommodate the progressive necking
716 of a continental lithosphere up to mantle exhumation. The conceptual model shown in figure
717 10 summarizes our field observations and measurements in three steps that directly result
718 from the three major thermo-mechanical changes that occur during necking of a continental
719 lithosphere: i) the reversal of shear sense with depth is controlled by the initial two-peak
720 strength profile of the lithosphere, ii) extremely strong stretching in the central zone of the
721 lithosphere neck results from the intense strain localization in the subcontinental mantle, and

722 iii) the late steep normal faults that crosscut both crust and mantle result from fast cooling in
723 the zone of hyper-stretching.

724

725 This progressive deformation pattern that characterizes mantle exhumation in the
726 western Betics (Figs. 11e and f) can be compared with end-member mechanical models in
727 which the bulk deformation is either i) rather symmetrical as a result of an efficient
728 decoupling between the upper crust and lithospheric mantle along a crustal décollement (Figs.
729 11a and b, Brun and Beslier, 1996) or ii) starting symmetrical and becoming strongly
730 asymmetrical, controlled by one or more lithosphere-scale detachment(s) (Figs. 11c and d;
731 Mohn et al., 2012). For convenience, only the first stages of lithosphere necking and the last
732 stages of mantle exhumation are represented in Figure 11. The two models differ significantly
733 not only in terms of bulk structural symmetry but also considering the role played by ductile
734 deformation.

735

736 In the symmetrical necking model (Figs. 11a and b, Brun and Beslier, 1996) the
737 middle ductile crust (décollement) is sheared top to the rift axis. In the lithospheric mantle,
738 ductile shear is localized below the high strength mantle layer with a sense of shear top away
739 from the rift axis. During increasing extension, the thinning and rupture of the sub-Moho
740 high-strength layer brings into contact the crust and mantle shear zones with their opposite
741 senses of shear. The exhumed mantle only displays the sense of shear top away from rift
742 center. In this process the same pattern of ductile shear affects the two rift margins even if the
743 continental breakup does not occur at the center of the rift zone. In other words, a difference
744 in bulk margin shape (i.e. width and thickness gradient) does not necessarily imply a strong
745 internal asymmetry in terms of structure and kinematics.

746

747 In the asymmetrical hyperextension model (Figs. 11c and d, Mohn et al., 2012), even
748 if rifting starts rather symmetrical, a strong asymmetry characterizes the final structure and
749 deformation pattern. This model implies an excision i) of the middle crust (Mohn et al., 2012)
750 or ii) of the high strength lithospheric mantle (Whitmarsh et al., 2001) or iii) of both
751 middle crust and lithospheric mantle (Lavier and Manatschal, 2006). From a kinematic point
752 of view, this model is characterized by a single sense of shear top-to-detachment hanging wall
753 from the upper crust to the ductile mantle (Lavier and Manatschal, 2006; Whitmarsh et al.,
754 2001). Finally and more importantly, in terms of model prediction, the two conjugate margins
755 in this model, correspond to the hanging-wall and footwall of a lithosphere-scale detachment,
756 respectively. Consequently, they must have strikingly different lithosphere-scale structures
757 and deformation patterns.

758
759 The pattern of deformation associated to mantle exhumation in the western Betics
760 (Figs. 11 e and f) has three important outcomes. First, it provides, for the first time, field
761 evidence of a vertical reversal of shear sense as predicted by the laboratory experiments of
762 Brun and Beslier (1996) (Fig. 11a). Second, it shows that crustal layers first underwent a
763 strong thinning, by simultaneous faulting in the upper crust and ductile shear in the middle
764 crust, during which extremely high values of stretching were reached prior to full mantle
765 exhumation. Third, full mantle exhumation was accommodated by newly formed high-angle
766 normal faults, cutting through the strongly thinned middle-lower crust and the underlying
767 brittle mantle, and block tilting. One can expect that, if extension would not have been
768 interrupted by rift inversion, the normal faulting and block tilting would have continued in a
769 core complex exhumation mode of the underlying ductile mantle (Fig. 11f). Mantle
770 detachment faults are thus more likely very late structures of the necking process.

771

772

773 **6/ Conclusions**

774

775 Our study that links field geology and geochronology leads to the following conclusions:

776

777 1/ The western Betics presents an exceptional exposure of a hyper-stretched continental
778 lithosphere section, which includes the world largest subcontinental mantle massif (Ronda
779 Peridotites), exhumed during the Oligocene-Lower Miocene in a back-arc tectonic setting.

780

781 2/ Variations in crustal thickness in the lithosphere section indicate amounts of stretching that
782 may locally reach values as high as 2400%, defining a stage of hyper-stretching.

783

784 3/ Ductile deformation associated to lithosphere thinning is marked by opposite senses of
785 shear in the lower crust/subcontinental mantle and in the upper/middle crust, highlighting a
786 mechanical decoupling between the upper crust and the localizing subcontinental mantle. The
787 presence of a high strength sub-Moho mantle is responsible for this change in sense of shear
788 with depth. Whereas mantle exhumation in the western Betics occurred in a backarc setting,
789 this deformation pattern, controlled by a high-strength layer at the top of the lithosphere
790 mantle, makes it directly comparable to most passive margin formation that have lead to
791 mantle exhumation. Therefore, this unique field example has a strong potential for the seismic
792 interpretation of the so-called “hyper-extended margins”.

793

794 4/ In the course of extension, the ductile crust almost disappeared in the hyper-stretched
795 segment (i.e. lithosphere neck) and the upper crust became mechanically coupled to the
796 underlying serpentized mantle.

797

798 5/ On the above bases, three main steps summarize the lithosphere necking process:

799 i/ a mid-crustal shear zone and a crust-mantle shear zone that acted synchronously but
800 with opposite senses of shear, accommodated ductile crust thinning and ascent of the
801 subcontinental mantle,

802 ii/ hyper-stretching localized in the lithosphere neck lead to an almost disappearance
803 of the ductile crust and brought the upper crust in contact with the subcontinental mantle, each
804 of them with their already acquired opposite senses of shear;

805 iii/ high-angle normal faulting cutting through the Moho and related block tilting
806 achieved the full exhumation of mantle in the domain of localized stretching.

807

808 **Aknowledgement**

809

810 This work was funded by the European Union FP7 Marie Curie ITN “TOPOMOD”,
811 contract 264517. Thanks to Alexandre Pichat and Hugo Humbert for help in the field.
812 Constructive reviews by Tony Doré and Geoffroy Mohn helped improve the manuscript.

813

814

815

816

817 **REFERENCES**

818

819 Afiri, A., Gueydan, F., Pitra, P., Essai, A., and Précigout, J. (2011). Oligo-miocene
820 exhumation of the Beni-Bousera peridotite through a lithosphere-scale extensional shear zone.
821 *Geodinamica Acta*, 24(1):49-60.

822

823 Aguado, R., Feinberg, H., Durand-Delga, M., Martín-Algarra, A., Esteras, M., and Didon, J.
824 (1990). Nuevos datos sobre la edad de las formaciones miocenas transgresivas sobre las
825 Zonas Internas Béticas : la Formación de San Pedro de Alcantara (Provincia de Málaga).
826 *Revista de la Sociedad Geológica de España*, 3(1-2):79-85.

827

828 Alcalá, F. J., F. Guerrero, F. M. Martín-Martín, M., Raffaelli, G., and Serrano F. (2014).
829 Geodynamic implications derived from Numidian-like distal turbidites deposited along the
830 Internal–External Domain Boundary of the Betic Cordillera (S Spain). *Terra Nova*, 25:119-
831 129.

832

833 Argles, T. and Platt, J. (1999). Stepped fibres in sillimanite-bearing veins: valid shear-sense
834 indicators in high grade rocks?. *Journal of Structural Geology*, 21(2):153-159.

835

836 Argles, T., Platt, J., and Waters, D. (1999). Attenuation and excision of a crustal section
837 during extensional exhumation: the Carratraca massif, Betic Cordillera, southern Spain.
838 *Journal of the Geological Society*, 156(1):149-162.

839

840 Balanyá, J. C., Crespo-Blanc, A., Díaz-Azpiroz, M., Exósito, I., and Luján, M. (2007).
841 Structural trend line pattern and strain partitioning around the Gibraltar arc accretionary

- 842 wedge: Insights as to the mode of orogenic arc building. *Tectonics*, 26(2):TC2005
- 843
- 844 Balanyá, J. C., García-Dueñas, V., Azañón, J. M., and Sánchez-Gómez, M. (1997).
- 845 Alternating contractional and extensional events in the Alpujarride nappes of the Alboran
- 846 domain (Betics, Gibraltar arc). *Tectonics*, 16(2):226-238.
- 847
- 848 Beltrando, M., Frasca, G., Compagnoni R. and Vitale Brovarone A. (2012). The Valaisan
- 849 controversy revisited: Multi-stage folding of Mesozoic hyper-extended margin in the Petit St.
- 850 Bernard Pass area. *Tectonophysics*. 579:17-36.
- 851
- 852 Berndt, T., Ruiz-Martínez, V. C., Chalouan, A. (2015). New constraints on the evolution of
- 853 the Gibraltar Arc from palaeomagnetic data of the Ceuta and Beni Bousera peridotites (Rif,
- 854 northern Africa). *Journal of Geodynamics*, 84:19-39.
- 855
- 856 Beslier, M.-O., Ask, M., and Boillot, G. (1993). Ocean-continent boundary in the Iberia
- 857 abyssal plain from multichannel seismic data. *Tectonophysics*, 218(4):383-393.
- 858
- 859 Beslier, M.-O., Girardeau, J., and Boillot, G. (1990). Kinematics of peridotite emplacement
- 860 during north Atlantic continental rifting, Galicia, northwestern Spain. *Tectonophysics*, 184(3):
- 861 321-343.
- 862
- 863 Blichert-Toft, J., Albarède, F., and Kornprobst, J. (1999). Lu-Hf isotope systematics of garnet
- 864 pyroxenites from Beni Bousera, Morocco: Implications for basalt origin: *Science*, 283:1303-
- 865 1306.
- 866

867 Boillot, G., Grimaud, S., Mauffret, A., Mougnot, D. Kornprobst, J., Mergoil, D. J., and
868 Torrent, G. (1980). Ocean continent boundary of the Iberian margin: A serpentinite diapir
869 west of the Galicia Bank. *Earth And Planetary Science Letters*, 48:23-34.

870

871 Boillot, G., Recq, M., Winterer, E.L., Meyer, A.W., Applegate, J., Baltuck, M., Bergen, J.A.,
872 Comas, M.C., Davies, T.A., Dunham, K., Evans, C.A., Girardeau, J., Goldberg, G., Haggerty,
873 J., Jansa, L.F., Johnson, J.A., Kasahara, J., Loreau, J.P., Luna-Sierra, E., Mollade, M., Ogg, J.,
874 Sarti, M., Thurow, J., and Williamson M. (1987). Tectonic Denudation Of The Upper Mantle
875 Along Passive Margin: A Model Based On Drilling Results (Odp Leg 103, Western Galicia
876 Margin, Spain). *Tectonophysics*, 132:335-342.

877

878 Bonnin, M., Nolet, G., Villaseñor, A., Gallart, J., and Thomas, C. (2014). Multiple-frequency
879 tomography of the upper mantle beneath the African/Iberian collision zone. *Geophysical*
880 *Journal International*, 198(3):1458-1473.

881

882 Bourgois, J. (1978). La transversale de Ronda (Cordillères Bétiques, Espagne). Données
883 géologiques pour un modèle d'évolution de l'Arc de Gibraltar. *Annales Scientifiques de*
884 *l'Université de Besançon (France)*, 30:1-445.

885

886 Bourgois, J., Chauve, P., Lorenz, C., Monnot, J., Peyre, Y., Rigo, E. and Rivière, M. (1972a).
887 La formation d'Alozaina. Série d'âge oligocène et aquitainien transgressive sur le Bétique de
888 Malaga. *C. R. Acad. Sci. Paris*, 275(D):531-534.

889

890 Bourgois, J., Chauve, P., Magne, J., Monnot, J., Peyre, Y., Rigo, E. and Rivière, M. (1972b).
891 La formation de Las Millanas. Série burdigalienne transgressive, sur les zones internes des

- 892 cordillères bétiques occidentales (région d'Alozaina-Tolox, province de Malaga, Espagne). C.
893 R. Acad. Sci. Paris, 275(D):169-172.
- 894
- 895 Brun, J.P. and Beslier, M.O. (1996). Mantle exhumation at passive margins. Earth and
896 Planetary Science Letters 142:161-173.
- 897
- 898 Cano Medina, F. and Ruiz Reig, P. (1990). Sheet Ardales, 1051. Geological map scale
899 1:50000, Instituto Geológico y Minero de España, Madrid.
- 900
- 901 Célérier, B. (2013). FSA: Fault & Stress Analysis software, version 35.1, [http://www.pages-](http://www.pages-perso-bernard-celerier.univ-montp2.fr/software/dcmt/fsa/fsa.html)
902 [perso-bernard-celerier.univ-montp2.fr/software/dcmt/fsa/fsa.html](http://www.pages-perso-bernard-celerier.univ-montp2.fr/software/dcmt/fsa/fsa.html).
- 903
- 904 Chalouan, A., Michard, A., El Kadiri, K., Frizon de Lamotte, D., Negro, F., Soto, J., and
905 Saddiqi, O. (2008). The Rif belt. In Michard, A., Saddiqi, O., Chalouan, A., de Lamotte, D.F.,
906 editors, Continental Evolution: The Geology of Morocco: Structure, Stratigraphy, and
907 Tectonics of the Africa–Atlantic–Mediterranean Triple Junction. Springer: 203-302.
- 908
- 909 Chamón Cobos, C., Quinquer Agut, R., Crespo, V., Aguilar, M., and Reyes, J.L. (1972).
910 Sheet Alora, 1052. Geological map scale 1:50000, Instituto Geológico y Minero de España,
911 Madrid.
- 912
- 913 Clerc, C., and Lagabrielle, Y. (2014). Thermal control on the modes of crustal thinning
914 leading to mantle exhumation: Insights from the Cretaceous Pyrenean hot paleomargins.
915 Tectonics, 33(7):1340-1359.
- 916

- 917 Clerc, C., Lagabrielle, Y., Neumaier, M., Reynaud, J.Y., de Saint Blanquat, M. (2012).
918 Exhumation of subcontinental mantle rocks: evidence from ultramafic-bearing clastic deposits
919 nearby the Lherz peridotite body, French Pyrenees. *Bulletin de la Société géologique de*
920 *France* 183(5):443-459.
- 921
- 922 Cochran, J.R., and Karner, G.D. (2007). Constraints on the deformation and rupturing of
923 continental lithosphere of the Red Sea: The transition from rifting to drifting. In Karner, G. D.,
924 Manatschal, G., Pinheiro, L. M., editors, *Imaging, Mapping and Modelling Continental*
925 *Lithosphere Extension and Breakup*. Geological Society, London, Special Publications,
926 282:265-289.
- 927
- 928 Comas, M. C., García-Dueñas, V., and Jurado, M. (1992). Neogene tectonic evolution of the
929 Alboran Sea from MCS data. *Geo-Marine Letters*, 12(2-3):157-164.
- 930
- 931 Comas, M. C., Platt, J. P., Soto, J. I., and Watts, A. B. (1999). The origin and tectonic history
932 of the Alboran basin: Insights from LEG 161 results. In Zahn, R., Comas, M. C. and Klaus, A.,
933 editors, *Proceedings of the Ocean Drilling Program, Scientific Results*:555-580.
- 934
- 935 Contrucci, I., Matias, L., Moulin, M., Geli, L., Klingelhofer, F., Nouze, H., Aslanian, D.,
936 Olivet, J.L., Rehault, J.P., and Sibuet, J.C. (2004). Deep structure of the West African
937 continental margin (Congo, Zaire, Angola), between 5°S and 8°S, from reflection/refraction
938 seismics and gravity data. *Geophysical Journal International*, 158:529-553.
- 939
- 940 Crespo-Blanc, A. and Campos, J. (2001). Structure and kinematics of the south iberian
941 paleomargin and its relationship with the Flysch Trough Units: extensional tectonics within

942 the Gibraltar arc fold-and-thrust belt (Western Betics). *Journal of Structural Geology*,
943 23(10):1615-1630.

944

945 Crespo-Blanc, A. and Frizon de Lamotte, D. (2006). Structural evolution of the external zones
946 derived from the Flysch Trough and the south iberian and maghrebien paleomargins around
947 the Gibraltar arc: a comparative study. *Bulletin de la Societé Géologique de France*,
948 177(5):267-282.

949

950 Cruz San Julián, J. (1990). Sheet Teba, 1037. Geological map scale 1:50000, Instituto
951 Geológico y Minero de España, Madrid.

952

953 Davies, G. R., Nixon, P. H., Pearson, D. G., and Obata, M. (1993). Tectonic implications of
954 graphitized diamonds from the ronda, peridotite massif, southern Spain. *Geology*, 21(5):471-
955 474.

956

957 Davis, M. and Kusznir, N. (2004). Depth-dependent lithospheric stretching at rifted
958 continental margins. *Proceedings of NSF Rifted Margins Theoretical Institute*, 136:1-92.

959

960 Del Olmo Sanz, A., Moreno Serrano, F., Campos Fernández, J., Estévez, A., García-Dueñas,
961 V., García-Rossell, L., Martín-Algarra, A., Orozco Fernández, M., and Sanz de Galdeano, C.
962 (1990). Sheet Ronda, 1051. Geological map scale 1:50000, Instituto Geológico y Minero de
963 España, Madrid.

964

965 Didon, J., Durand-Delga, M., and Kornprobst, J. (1973). Homologies géologiques entre les
966 deux rives du détroit de Gibraltar. *Bulletin de la Societé Géologique de France*, 15(2):77-105.

- 967
- 968 Doblas, M. and Oyarzun, R. (1989). Neogene extensional collapse in the Western
969 Mediterranean (Betic-Rif alpine orogenic belt): Implications for the genesis of the Gibraltar
970 arc and magmatic activity. *Geology*, 17(5):430-433.
- 971
- 972 Duggen, S., Hoernle, K., van den Bogaard, P., and Harris, C. (2004). Magmatic evolution of
973 the Alboran region: The role of subduction in forming the Western Mediterranean and
974 causing the Messinian salinity crisis. *Earth and Planetary Science Letters*, 218(1-2):91-108.
- 975
- 976 Esteban, J. J., Cuevas, J., Vegas, N., and Tubía, J. M. (2008). Deformation and kinematics in
977 a melt-bearing shear zone from the Western Betic Cordilleras (southern Spain). *Journal of*
978 *Structural Geology*, 30(3):380-393.
- 979
- 980 Esteban, J. J., Sánchez-Rodríguez, L., Seward, D., Cuevas, J., and Tubía, J. M. (2004). The
981 late thermal history of the Ronda area, southern Spain. *Tectonophysics*, 389(1-2):81-92.
- 982
- 983 Esteban, J.J., Cuevas, J., Tubía, J., Sergeev, S., and Larionov, A. (2011). A revised
984 Aquitanian age for the emplacement of the Ronda Peridotites (Betic Cordilleras, southern
985 Spain). *Geol. Mag.*, 148(1):183-187.
- 986
- 987 Esteban, J. J., Tubía, J. M., Cuevas, J., Seward, D., Larionov, A., Sergeev, S., and Navarro-
988 Vilá, F. (2013). Insights into extensional events in the Betic Cordilleras, southern Spain: New
989 fission-track and U-Pb SHRIMP analyses. *Tectonophysics*, 603:179-188.
- 990
- 991 Faccenna, C., Piromallo, C., Crespo Blanc, A., Jolivet, L., and Rossetti, F. (2004). Lateral

- 992 slab deformation and the origin of the arcs of the western Mediterranean. *Tectonics*,
993 23:TC1012.
- 994
- 995 Feinberg, H., Saddiqi, O., and Michard, A. (1996). New constraints on the bending of the
996 Gibraltar arc from paleomagnetism of the Ronda peridotite (Betic Cordilleras, Spain). In
997 Morris A., T. D., editor, *Paleomagnetism and Tectonics of the Mediterranean Region*, volume
998 105 of *Geol. Soc. Lond. Spec. Pubs*, The Geological Society, London:43-52.
- 999
- 1000 Fernández-Fernández, E.M., Jabaloy-Sánchez, A., Nieto, F., González-Lodeiro, F. (2007).
1001 Structure of the Maláguide Complex near Vélez Rubio (Eastern Betic Cordillera, SE Spain).
1002 *Tectonics*, 26:TC4008.
- 1003
- 1004 Fernández, M., Berástegui, X., Puig, C., García-Castellanos, D., Jurado, M. J., Torné, M., and
1005 Banks, C. (1998). Geophysical and geological constraints on the evolution of the
1006 Guadalquivir foreland basin, Spain. *Geological Society, London, Special Publications*,
1007 134(1):29-48.
- 1008
- 1009 Flinch J.F. (1993). *Tectonic evolution of the Gibraltar Arc*. PhD thesis, Rice University,
1010 Houston, Texas.
- 1011
- 1012 Frasca, G., Gueydan, F., and Brun, J. P. (2015). Structural record of Lower Miocene
1013 westward Alboran Domain motion in the Western Betics (southern Spain). *Tectonophysics*,
1014 657:1-20.
- 1015
- 1016 Frets, E. C., Tommasi, A., Garrido, C. J., Vauchez, A., Mainprice, D., Targuisti, K., and Amri,

- 1017 I. (2014). The Beni-Bousera peridotite (Rif belt, Morocco): an oblique-slip low-angle shear
1018 zone thinning the subcontinental mantle lithosphere. *Journal of Petrology*, 55(2):283-313.
1019
- 1020 Frizon de Lamotte, D. F., Leturmy, P., Missenard, Y., Khomsi, S., Ruiz, G., Saddiqi, O.,
1021 Guillocheau, F., and Michard, A. (2009). Mesozoic and cenozoic vertical movements in the
1022 atlas system (Algeria, Morocco, Tunisia): An overview. *Tectonophysics*, 475(1):9-28.
1023
- 1024 Froitzheim, N., Pleuger, J., and Nagel, T.J. (2006). Extraction faults. *Journal of Structural*
1025 *Geology*, 28:1388-1395.
1026
- 1027 García-Dueñas, V., Balanyá, J. C., and Martínez-Martínez, J. (1992). Miocene extensional
1028 detachments in the outcropping basement of the northern Alboran basin (Betics) and their
1029 tectonic implications. *Geo-Marine Letters*, 12:88-95.
1030
- 1031 Garrido, C. J. and Bodinier, J.-L. (1999). Diversity of mafic rocks in the Ronda Peridotite:
1032 Evidence for pervasive melt–rock reaction during heating of subcontinental lithosphere by
1033 upwelling asthenosphere. *Journal of Petrology*, 40(5): 729-754.
1034
- 1035 Garrido, C. J., Gueydan, F., Booth-Rea, G., Précigout, J., Hidas, K., Padrón-Navarta, J. A.,
1036 and Marchesi, C. (2011). Garnet lherzolite and garnet-spinel mylonite in the Ronda peridotite:
1037 Vestiges of Oligocene backarc mantle lithospheric extension in the Western Mediterranean.
1038 *Geology*, 39(10):927-930.
1039
- 1040 Gueguen, E., Doglioni, C., and Fernández, M. (1998). On the post-25 Ma geodynamic
1041 evolution of the Western Mediterranean. *Tectonophysics*, 298(1-3):259-269.

- 1042
- 1043 Gueydan, F., Morency, C., and Brun, J.-P. (2008). Continental rifting as a function of
1044 lithosphere mantle strength. *Tectonophysics*, 460(1-4):83-93.
- 1045
- 1046 Gueydan, F. and Précigout, J. (2014). Modes of continental rifting as a function of ductile
1047 strain localization in the lithospheric mantle. *Tectonophysics*, 612-613:18-25.
- 1048
- 1049 Gueydan, F., Précigout, J., and Montési, L. G. J. (2014). Strain weakening enables continental
1050 plate tectonics. *Tectonophysics*, 63:189-196.
- 1051
- 1052 Gueydan, F., Pitra P., Afiri, A., Poujol, M., Essaifi, A., and Paquette, J.-L. (2015). Oligo-
1053 Miocene thinning of the Beni Bousera peridotites and their Variscan crustal host rocks,
1054 Internal Rif, Morocco. *Tectonics*, 34:1244-1268.
- 1055
- 1056 Gutscher, M.-A., Malod, J., Rehault, J.-P., Contrucci, I., Klingelhoefer, F., Mendes-Victor, L.,
1057 and Spakman, W. (2002). Evidence for active subduction beneath Gibraltar. *Geology*,
1058 30:1071-1074.
- 1059
- 1060 Hidas, K., Booth-Rea, G., Garrido, C. J., Martínez-Martínez, J. M., Padrón-Navarta, J. A.,
1061 Konc, Z., Giaconia, F., Frets, E., and Marchesi, C. (2013). Backarc basin inversion and
1062 subcontinental mantle emplacement in the crust: kilometre-scale folding and shearing at the
1063 base of the proto-Alborán lithospheric mantle (Betic Cordillera, southern Spain). *Journal of*
1064 *the Geological Society*, 170(1):47-55.
- 1065
- 1066 Hidas, K., Varas-Reus, M. I., Garrido, C. J., Marchesi, C., Acosta-Vigil, A., Padrón-Navarta,

1067 J. A., Targuisti, K., and Konc, Z. (2015). Hyperextension of continental to oceanic-like
1068 lithosphere: The record of late gabbros in the shallow subcontinental lithospheric mantle of
1069 the westernmost Mediterranean. *Tectonophysics*, 650:65-79.

1070

1071 Huismans, R. S. Beaumont, C. (2011). Depth-dependent extension, two-stage breakup and
1072 cratonic underplating at rifted margins. *Nature*, 473:74-78.

1073

1074 Insua-Arévalo, J.M., Martínez-Díaz, J.J., García-Mayordomo, J., and Martín-González, F.
1075 (2012). Active tectonics in the Malaga Basin: evidences from morphotectonic markers
1076 (Western Betic Cordillera, Spain). *Journal of Iberian Geology*, 38(1):175-190.

1077

1078 Iribarren, L., Vergés, J., and Fernández, M. (2009). Sediment supply from the Betic-Rif
1079 orogen to basins through Neogene. *Tectonophysics*, 475(1):68-84.

1080

1081 Johanesen, K. E. and Platt, J. P. (2015). Rheology, microstructure, and fabric in a large scale
1082 mantle shear zone, Ronda Peridotite, Southern Spain. *Journal of Structural Geology*, 73:1-17.

1083

1084 Johanesen, K., Platt, J. P., Kaplan, M. S., and Ianno, A. J. (2014). A revised thermal history of
1085 the Ronda Peridotite, S. Spain: New evidence for excision during exhumation. *Earth and
1086 Planetary Science Letters*, 393:187-199.

1087

1088 Kornprobst, J. (1976). Signification structurale des péridotites dans l'orogène Bético-Rifain:
1089 arguments tirés de l'étude des détritiques observés dans les sédiments Paléozoïque. *Bulletin de la
1090 Société Géologique de France*, 3:607-618.

1091

- 1092 Lavier, L. L. and Manatschal, G. (2006). A mechanism to thin the continental lithosphere at
1093 magma-poor margins. *Nature*, 440(7082):324–328.
- 1094
- 1095 Lenoir, X., Garrido, C.J., Bodinier, J.L., Dautria, J.M., and Gervilla, F. (2001). The
1096 recrystallization front of the Ronda peridotite: Evidence for melting and thermal erosion of
1097 subcontinental lithospheric mantle beneath the Alboran basin: *Journal of Petrology*, 42:141-
1098 158.
- 1099
- 1100 Lister, G., Etheridge, M., and Symonds, P. (1986). Detachment faulting and the evolution of
1101 passive continental margins. *Geology*, 14(3):246–250.
- 1102
- 1103 Lonergan, L. and White, N. (1997). Origin of the Betic-Rif mountain belt. *Tectonics*, 16:504-
1104 522.
- 1105
- 1106 López-Garrido, A. C. and Sanz de Galdeano, C. (1999). Neogene sedimentation and tectonic-
1107 eustatic control of the Malaga basin, south Spain. *Journal of Petroleum Geology*, 22(1):81-96.
- 1108
- 1109 Manatschal, G. (2004). New models for evolution of magma-poor rifted margins based on a
1110 review of data and concepts from West Iberia and the Alps. *International Journal of Earth*
1111 *Sciences*, 93:432-466.
- 1112
- 1113 Manatschal, G., Froitzheim, N., Rubenach, M., and Turrin, B. (2001). The role of detachment
1114 faulting in the formation of an ocean-continent transition: insights from the Iberia abyssal
1115 plain. *Geological Society, London, Special Publications*, 187(1):405-428.
- 1116

- 1117 Marchesi, C., Garrido, C. J., Bosch, D., Bodinier, J.-L., Hidas, K., Padrón-Navarta, J.A., and
1118 Gervilla, F. (2012). A late Oligocene suprasubduction setting in the westernmost
1119 Mediterranean revealed by intrusive pyroxenite dikes in the Ronda Peridotite (southern
1120 Spain): *The Journal of Geology*, 120(2):237-247.
- 1121
- 1122 Martín-Algarra, A. (1987). Evolución geológica alpina del contacto entre las Zonas Internas y
1123 las Zonas Externas de la Cordillera Bética. PhD thesis, Universidad de Granada.
- 1124
- 1125 Mazzoli, S. and Martín-Algarra, A. (2011). Deformation partitioning during transpressional
1126 emplacement of a 'mantle extrusion wedge': the Ronda peridotites, Western Betic Cordillera,
1127 Spain. *Journal of the Geological Society of London*, 168:373-382.
- 1128
- 1129 Mazzoli, S., Martín-Algarra, A., Reddy, S., Sánchez-Vizcaíno, V. L., Fedele, L., and Noviello,
1130 A. (2013). The evolution of the footwall to the Ronda subcontinental mantle peridotites:
1131 insights from the Nieves Unit (Western Betic Cordillera). *Journal of the Geological Society of*
1132 *London*, 170:385-402.
- 1133
- 1134 Mohn G., Manatschal G., Müntener O., Beltrando M., Masini E. (2010). Unravelling The
1135 Interaction Between Tectonic And Sedimentary Processes During Lithospheric Thinning In
1136 The Alpine Tethys Margins. *Int. J. Earth Sci.*, 99:75-101.
- 1137
- 1138 Mohn, G., Manatschal, G., Beltrando, M., Masini, E., Kuszniir, N. (2012). Necking of
1139 continental crust in magma-poor rifted margins: evidence from the fossil Alpine Tethys
1140 margins. *Tectonics*, 31:TC2961.
- 1141

- 1142 Monié, P., Torres-Roldán, R., and García-Casco, A. (1994). Cooling and exhumation of the
1143 Western Betic Cordillera, $^{40}\text{Ar}/^{39}\text{Ar}$ thermochronological constraints on a collapsed terrane.
1144 *Tectonophysics*, 238(1-4):353-379.
- 1145
- 1146 Montel, J.-M., Kornprobst, J., and Vielzeuf, D. (2000). Preservation of old U-Th-Pb ages in
1147 shielded monazite: example from the Beni-Bousera hercynian kinzigites (Morocco). *Journal*
1148 *of Metamorphic Geology*, 18(3):335-342.
- 1149
- 1150 Moulin M., Aslanian D., Olivet J.L., Klingelhoefer F., Nouzé H., Rehault J.P., Unterneuh P.
1151 (2005). Geological constraints on the evolution of the angolan margin based on reflection and
1152 refraction seismic data (Zaïango Project). *Geophys. J. Int.*, 162:793-810.
- 1153
- 1154 Nagel, T. J. and Buck, W. R. (2004). Symmetric alternative to asymmetric rifting models.
1155 *Geology*, 32(11):937-940.
- 1156
- 1157 Navarro-Vilá, F. and Tubía, J. (1983). Essai d'une nouvelle différenciation des nappes
1158 Alpujarrides dans le secteur occidental des Cordillères Bétiques (Andalousie, Espagne). *C. R.*
1159 *Acad. Sci. Paris*, 296:111-114.
- 1160
- 1161 Negro, F., Beyssac, O., Goffé, B., Saddiqi, O., and Bouybaouéne, M. L. (2006). Thermal
1162 structure of the Alboran Domain in the Rif (northern Morocco) and the Western Betics
1163 (southern Spain). Constraints from Raman spectroscopy of carbonaceous material. *Journal of*
1164 *Metamorphic Geology*, 24 (4):309-327.
- 1165
- 1166 Obata, M. (1980). The Ronda peridotite: garnet-, spinel-, and plagioclase-lherzolite facies and

- 1167 the P-T trajectories of a high-temperature mantle intrusion. *Journal of Petrology*, 21(3):533-
1168 572.
- 1169
- 1170 Osmundsen, P. T., and Ebbing, J. (2008). Styles of extension offshore mid-Norway and
1171 implications for mechanisms of crustal thinning at passive margins. *Tectonics*, 27:TC6016.
- 1172
- 1173 Palomeras, I., Thurner, S., Levander, A., Liu, K., Villasenor, A., Carbonell, R., and Harnafi,
1174 M. (2014). Finite-frequency Rayleigh wave tomography of the western Mediterranean:
1175 Mapping its lithospheric structure. *Geochemistry, Geophysics, Geosystems*, 15(1):140-160.
- 1176
- 1177 Pearson, D.G., Davies, G.R., Nixon, P.H., and Milledge, H.J. (1989). Graphitized diamonds
1178 from a peridotite massif in Morocco and implications for anomalous diamond occurrences:
1179 *Nature*, 335:60-63.
- 1180
- 1181 Pearson, D.G. and Nowell, G.M. (2004). Re-Os and Lu-Hf isotope constraints on the origin
1182 and age of pyroxenites from the Beni Bousera peridotite massif implications for mixed
1183 peridotite pyroxenite mantle sources. *Journal of Petrology*, 45: 439-455.
- 1184
- 1185 Péron-Pinvidic, G. and Manatschal, G. (2009). The Final Rifting Evolution At Deep Magma-
1186 Poor Passive Margins From Iberia-Newfoundland: A New Point Of View. *Int. J. Earth Sci.*,
1187 98:1581-1597.
- 1188
- 1189 Péron-Pinvidic, G., Manatschal, G., Minshull, T. A. and Sawyer, D. S. (2007).
1190 Tectonosedimentary evolution of the deep Iberia-Newfoundland margins: Evidence for a
1191 complex breakup history. *Tectonics*, 26:1-29.

- 1192
- 1193 Peyre, Y. (1974). Géologie d'Antequera et de la région Cordillères Bétiques (Espagne). PhD
1194 thesis, University of Paris, France. 528 pp.
- 1195
- 1196 Platt, J. P., Allerton, S., Kirker, A., and Platzman, E. (1995). Origin of the western subbetic
1197 arc (south Spain): palaeomagnetic and structural evidence. *Journal of Structural Geology*,
1198 17(6):765–775.
- 1199
- 1200 Platt, J. P., Argles, T., Carter, A., Kelley, S., Whitehouse, M., and Lonergan, L. (2003a).
1201 Exhumation of the Ronda peridotite and its crustal envelope: constraints from thermal
1202 modelling of a P-T-time array. *Journal of the Geological Society*, 160(5):655-676.
- 1203
- 1204 Platt, J. P., Behr, W. M., Johanesen, K., and Williams, J. R. (2013). The Betic-Rif arc and its
1205 orogenic hinterland: A review. *Annual Review of Earth and Planetary Sciences*, 41(1):313-
1206 357.
- 1207
- 1208 Platt, J. P., and Whitehouse, M. (1999). Early Miocene high-temperature metamorphism and
1209 rapid exhumation in the Betic Cordillera (Spain): evidence from U-Pb zircon ages. *Earth and
1210 Planetary Science Letters*, 171(4):591-605.
- 1211
- 1212 Platt, J. P., Whitehouse, M., Kelley, S., Carter, A., and Hollick, L. (2003b). Simultaneous
1213 extensional exhumation across the Alboran Basin: implications for the causes of late orogenic
1214 extension. *Geology*, 31(3):251-254.
- 1215
- 1216 Précigout, J., Gueydan, F., Gapais, D., Garrido, C., and Essaifi, A. (2007). Strain localisation

- 1217 in the subcontinental mantle - a ductile alternative to the brittle mantle. *Tectonophysics*,
1218 445(3-4):318-336.
- 1219
- 1220 Précigout, J., Gueydan, F., Garrido, C. J., Cogné, N., and Booth-Rea, G. (2013). Deformation
1221 and exhumation of the Ronda peridotite (Spain). *Tectonics*, 32(4):1011-1025.
- 1222
- 1223 Ranero, C., and Pérez-Gussinyé, M. (2010). Sequential faulting explains the asymmetry and
1224 extension discrepancy of conjugate margins: *Nature*, 468(7321): 294-299.
- 1225
- 1226 Reston, T.J. (2007). The extension discrepancy at North Atlantic non-volcanic rifted margins:
1227 depth-dependent stretching or unrecognised faulting?: *Geology*, 35 :367-370.
- 1228
- 1229 Rosenbaum, G. and Lister, G. S. (2004). Formation of arcuate orogenic belts in the western
1230 Mediterranean region. *Geological Society of America Special Papers*, 383:41-56.
- 1231
- 1232 Royden, L. H. (1993). Evolution of retreating subduction boundaries formed during
1233 continental collision. *Tectonics*, 12:629-638.
- 1234
- 1235 Ruiz Cruz, M. D. and Sanz de Galdeano, C. (2014). Garnet variety and zircon ages in UHP
1236 meta-sedimentary rocks from the Jubrique Zone (Alpujárride complex, Betic Cordillera,
1237 Spain): evidence for a pre-alpine emplacement of the Ronda Peridotites. *International*
1238 *Geology Review*, 56(7):845-868.
- 1239
- 1240 Sánchez-Gómez, M., Azañón, J. M., García-Dueñas, V., and Soto, J. I. (1999). Correlation
1241 between metamorphic rocks recovered from site 976 and the Alpujárride rocks of the Western

- 1242 Betics. In Zahn, R., Comas, M. C. and Klaus, A., editors, Proceedings of the Ocean Drilling
1243 Program, Scientific Results:307-317.
- 1244
- 1245 Sánchez-Gómez, M., Balanyá, J. C., García-Dueñas, V., and Azañón, J. M. (2002).
1246 Intracrustal tectonic evolution of large lithosphere mantle slabs in the western end of the
1247 Mediterranean orogen (Gibraltar arc). *Journal of the Virtual Explorer*, 8:23-34.
- 1248
- 1249 Sánchez-Navas, A., García-Casco, A. and Martín-Algarra, A. (2014). Pre-Alpine discordant
1250 granitic dikes in the metamorphic core of the Betic Cordillera: tectonic implications. *Terra*
1251 *Nova*, 26(6):477-486.
- 1252
- 1253 Sánchez-Rodríguez, L. and Gebauer, D. (2000). Mesozoic formation of pyroxenites and
1254 gabbros in the Ronda area (southern Spain), followed by Early Miocene subduction
1255 metamorphism and emplacement into the middle crust: U-Pb sensitive high-resolution ion
1256 microprobe dating of zircon. *Tectonophysics*, 316(1-2):19-44.
- 1257
- 1258 Sanz de Galdeano, C., Serrano, F., López-Garrido, A. C. and Martín-Pérez, J. A. (1993).
1259 Paleogeography of the Late Aquitanian-Early Burdigalian Basin in the Western Betic internal
1260 zone. *Geobios*, 26(1):43-55.
- 1261
- 1262 Serrano, F., Guerra-Merchán, A., Kadiri, K. E., Sanz de Galdeano, C., López-Garrido, A. C.,
1263 Martín-Martín, M., and Hlila, R. (2007). Tectono-sedimentary setting of the Oligocene-Early
1264 Miocene deposits on the Betic-Rifian Internal Zone (Spain and Morocco). *Geobios*,
1265 40(2):191-205.
- 1266

- 1267 Soto, J. I. and Gervilla, F. (1991). Los macizos ultramáficos de Sierra de las Aguas y Sierra
1268 de la Robla como una ventana extensional (Béticas occidentales). *Geogaceta*, 9, 21-23.
1269
- 1270 Soustelle, V., Tommasi, A., Bodinier, J.L., Garrido, C.J., Vauchez, A. (2009). Deformation
1271 and reactive melt transport in the mantle lithosphere above a large-scale partial melting
1272 domain: the Ronda Peridotite Massif, southern Spain. *J. Petrol.* 50:1235-1266.
1273
- 1274 Suades, E. and Crespo-Blanc, A. (2013). Gravitational dismantling of the Miocene mountain
1275 front of the Gibraltar Arc system deduced from the analysis of an olistostromic complex.
1276 *Geologica Acta*, 11(2):215-229.
1277
- 1278 Torres-Roldán, R. L. (1979). The tectonic subdivision of the betic zone (betic cordilleras,
1279 south- ern spain); its significance and one possible geotectonic scenario for the westernmost
1280 alpine belt. *American Journal of Science*, 279(1):19–51.
1281
- 1282 Torres-Roldán, R.L., Poli, G., Peccerillo, A. (1986). An Early Miocene arc-tholeiitic
1283 magmatic dike event from the Alboran Sea - Evidence for precollisional subduction and back-
1284 arc crustal extension in the westernmost Mediterranean. *Geologische Rundschau*, 75:219–234.
1285
- 1286 Tubía, J., Cuevas, J., and Esteban, J. (2004). Tectonic evidence in the Ronda Peridotites,
1287 Spain, for mantle diapirism related to delamination. *Geology*, 32(11):941-944.
1288
- 1289 Tubía, J., Cuevas, J., and Esteban, J. (2013). Localization of deformation and kinematic shift
1290 during the hot emplacement of the ronda peridotites (Betic Cordilleras, southern Spain).
1291 *Journal of Structural Geology*, 50:148-160.

- 1292
- 1293 Tubía, J., Cuevas, J., and Ibarra, J. G. (1997). Sequential development of the metamorphic
1294 aureole beneath the Ronda peridotites and its bearing on the tectonic evolution of the Betic
1295 Cordillera. *Tectonophysics*, 279(1):227-252.
- 1296
- 1297 Tubía, J., Cuevas, J., Navarro-Vilá, F., Alvarez, F., and Aldaya, F. (1992). Tectonic evolution
1298 of the Alpujárride complex (Betic Cordillera, southern Spain). *Journal of structural geology*,
1299 14(2):193-203.
- 1300
- 1301 Tubía, J.M., Cuevas, J. (1986). High-temperature emplacement of the Los Reales peridotite
1302 nappe (Betic Cordillera, Spain). *Journal of Structural Geology* 8:473-482.
- 1303
- 1304 Turner, S., Platt, J., George, R., Kelley, S., Pearson, D., and Nowell, G. (1999). Magmatism
1305 associated with orogenic collapse of the betic-alboran domain, se spain. *Journal of Petrology*,
1306 40(6):1011-1036.
- 1307
- 1308 Van der Wal, D. and Vissers, R. L. M. (1993). Uplift and emplacement of upper mantle rocks
1309 in the Western Mediterranean. *Geology*, 21(12):1119-1122.
- 1310
- 1311 Van der Wal, D. and Vissers, R. L. M. (1996). Structural petrology of the Ronda Peridotite,
1312 SW Spain: Deformation history. *Journal of Petrology*, 37(1):23-43.
- 1313
- 1314 Van Hinsbergen, D. J. J., Vissers, R. L. M., and Spakman, W. (2014). Origin and
1315 consequences of Western Mediterranean subduction, rollback, and slab segmentation.
1316 *Tectonics*, 33(4):393-419.

- 1317
- 1318 Vergés, J. and Fernández, M. (2012). Tethys-Atlantic interaction along the Iberia-Africa plate
1319 boundary: The Betic-Rif orogenic system. *Tectonophysics*, 579(5):144-172.
- 1320
- 1321 Villasante-Marcos, V., Osete, M., Gervilla, F., and García-Dueñas, V. (2003). Palaeomagnetic
1322 study of the Ronda peridotites (Betic Cordillera, southern Spain). *Tectonophysics*,
1323 377(1):119-141.
- 1324
- 1325 Vissers, R. L. M., Platt, J. P., and van der Wal, D. (1995). Late orogenic extension of the
1326 Betic Cordillera and the Alboran domain: A lithospheric view. *Tectonics*, 14:786-803.
- 1327
- 1328 Watts, A., Platt, J. P., and Buhl, P. (1993). Tectonic evolution of the Alboran sea basin. *Basin*
1329 *Research*, 5:153-177.
- 1330
- 1331 Whitehouse, M. and Platt, J. (2003). Dating high-grade metamorphism - constraints from
1332 rare-earth elements in zircon and garnet. *Contributions to Mineralogy and Petrology*,
1333 145(1):61-74.
- 1334
- 1335 Whitmarsh, R. B. and Miles, P. R. (1995). Models of the development of the west Iberia rifted
1336 continental margin at 40°30' N deduced from surface and deep-tow magnetic anomalies.
1337 *Journal of Geophysical Research: Solid Earth*, 100(B3):3789-3806.
- 1338
- 1339 Whitmarsh, R. B., Manatschal, G., and Minshull, T. A. (2001). Evolution of magma-poor
1340 continental margins from rifting to seafloor spreading. *Nature*, 413:150-154.
- 1341

1342 Wilson, R. C. L., Manatschal, G. and Wise S. (2001). Rifting along non-volcanic passive
1343 margins: Stratigraphic and seismic evidence from the Mesozoic successions of the Alps and
1344 western Iberia. In R. C. L. Wilson, R. B. Whitmarsh, B. Taylor and N. Froitzheim, editors,
1345 Non-volcanic Rifting of Continental Margins: A Comparison of Evidence From Land and Sea.
1346 Geol. Soc. Spec. Publ., 187: 429-452.

1347
1348 Wortel, M. J. R. and Spakman, W. (2000). Subduction and slab detachment in the
1349 Mediterranean-Carpathian region. *Science*, 209:1910-1917.

1350
1351 Zindler, A., Staudigel, H., Hart, S.R., Endres, R., and Goldstein, S. (1983). Nd and Sm
1352 isotopic study of a mafic layer from Ronda ultramafic complex. *Nature*, 304:226-230.

1353
1354

1355 **Figure captions**

1356
1357 **Fig. 1. a)** Tectonic map of the Western Betics with foliation trajectories (modified after Frasca et al.
1358 2015) showing the main geological units: Ronda peridotites with plagioclase tectonites (dark green
1359 and pale green), lower, middle and upper crustal rocks above the peridotites (violet, dark brown and
1360 pale brown), crustal rocks below the peridotites (pale blue), lower Miocene Alzaina basin (beige) and
1361 Tortonian basins (pale yellow). Major tectonic contacts: Ronda Peridotites Thrust (RPT), Internal-
1362 External Zone Boundary (IEZB), crust-mantle extensional shear zone (white line). Top left inset:
1363 Location of the study area in the Betic-Rif belt with the location of the Ronda-Beni Bousera mantle
1364 bodies. Bottom right inset: synthetic vertical section of the lithological and tectonic units of the
1365 Western Betics. **b)** E-W trending cross-section; see location AA' in (a).

1366
1367 **Fig. 2. (a)** Subduction slab rollback setting of the Ronda peridotites in the Alboran domain, showing

1368 the present day geometry of the trench and its hypothetical position at 30 Ma. **(b)** Rifting at the front
1369 of the subduction upper plate responsible for mantle exhumation. **(c)** Rift inversion and thrust
1370 emplacement of the Ronda Peridotites on top of the Iberian margin (modified after Précigout et al.,
1371 2013).

1372
1373 **Fig. 3.** **(a)** Structural map of the Carratraca peridotitic massives (synthesized after Chamón Cobos et
1374 al., 1972; Cano Medina and Ruiz Reig, 1990; Cruz San Julián, 1990; Del Olmo Sanz et al., 1990; Soto
1375 and Gervilla, 1991; Argles et al., 1999; Tubía et al., 2004 and Frasca et al., 2015). Green star: position
1376 of the sample (GFD7) collected for the $^{40}\text{Ar}/^{39}\text{Ar}$ dating. LGFZ: Los Grenadillos Fault Zone. **(b)** NS
1377 cross-section showing the geometry of the three blocks of Sierra Agua, Sierra de la Robla and
1378 Alozaina. See location in (a).

1379
1380 **Fig. 4.** Kinematics and age of high-angle normal faults. **(a)** Outcrop photograph of the Cerro Tajo fault
1381 that put in contact middle crust gneisses with serpentized mantle rocks **(b)** Hand-specimen (GFD7)
1382 of the fault breccia sampled for $^{40}\text{Ar}/^{39}\text{Ar}$ dating (see location in Fig. 3.3a). White arrow: clast of the
1383 gneiss protolith containing only biotite. **(c)** Thin-section of sample GFD7 showing the formation of
1384 white mica pseudomorph after garnet. White arrow: very small white micas in the matrix (for details
1385 see “supplementary material”, Fig. S3). **(d and e)** Stereoplots of fault surfaces (lower hemisphere
1386 projection on a Schmidt net; FSA software by Célérier, 2013: version 35.2) for Cerro Tajo fault and
1387 La Robla fault (e) (see location of the faults in Fig. 3.3a). Great circles: fault planes. Grey arrows:
1388 direction of motion on fault surfaces. **(f)** $^{40}\text{Ar}/^{39}\text{Ar}$ age spectrum for the mm-sized white micas
1389 extracted from the sample GFD7 (see method and analytical data in “supplementary material”).

1390 **Fig. 5.** Types of shear indicators used in crust and mantle rocks **(a)** Landscape view (from point 5a in
1391 Fig. 4) of the thinned lithosphere in the Sierra de Agua. Left inset: Summary of senses of shear at the
1392 different lithosphere levels (not to scale; green: mantle; violet: lower crust; dark brown: middle crust;
1393 light brown: upper crust) with location of photographs (see location in Fig. 4). **(b)** Top-to-W sense of
1394 shear in the mantle: deflection of a pyroxenite layer in the Grt-Sp mylonitic foliation. **(c)** Top-to-W

1395 sense of shear in the lower crust: melt in veins and in pressure shadows around a garnet porphyroclasts
1396 and C'-type shear-bands, locally enriched in melt, in molten granulites. **(d)** Top-to-W sense of shear in
1397 the middle crust: sigmoidal stretched leucosome. **(e)** Top-to-E sense of shear in the middle crust:
1398 sigmoidal stretched leucosome. **(f)** Eyed-type section of a sheath fold in the middle crust in the
1399 sillimanite gneisses. **(g)** Top-to-E sense of shear in the middle/upper crust: C'-type brittle-ductile
1400 shear bands in the andalusite schists.

1401
1402 **Fig. 6.** Map of mean senses of shear in the Carratraca area. Colors of geological units like in Fig. 3.
1403 Ductile shear in the mantle and lower crust (Violet arrows) and in the middle crust (Blue arrows).
1404 Brittle/ductile shear, mainly observed in the upper crust (Pale blue) (For the whole set of lineation and
1405 shear criteria see "supplementary material", Fig. S1).

1406
1407 **Fig. 7.** Variations in crustal thickness. **(a)** Crustal thickness estimates in the Agua, La Robla and
1408 Aozaina blocks (green: mantle; violet: lower crust; dark brown: middle crust; light brown: upper
1409 crust) (See location in Fig. 3). **(b)** Estimates of the average thickness of the upper, middle and lower
1410 crust in the three blocks, made from local cross-sections that take into account variations in mean
1411 foliation dip.

1412
1413 **Fig. 8.** Low-angle normal fault (LANF) in the hyper-stretched portion of the rift (El Chenil area; see
1414 location in Fig. 6). **(a)** Landscape view of the El Chenil LANF. **(b)** Geological interpretation of the El
1415 Chenil fault zone (for detailed map and measurements see Fig. S2). **(c)** Photograph of ophicalcite.
1416 **(d)** Fault gouge in the fault core zone with clasts of quartz-veins (Q), breccia (B) and gneiss (G). **(e)**
1417 C'-type shear bands (shown by blue arrows) in the upper crustal rocks indicating a top-to-E sense of
1418 shear. **(f)** Sedimentary breccia at the base of the Aozaina basin with clasts of upper crustal rocks.

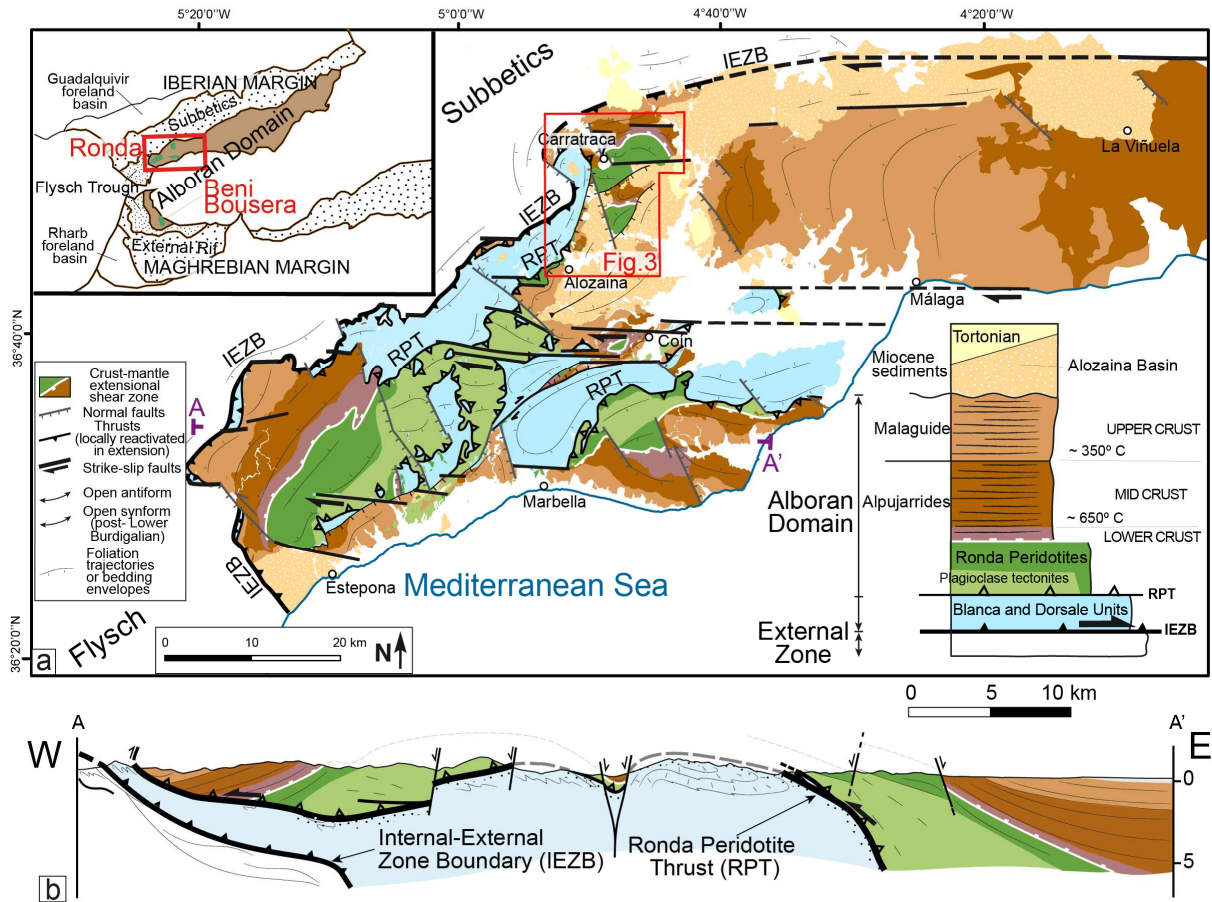
1419
1420 **Fig. 9.** Summary of shear sense variations with depth and their implications in terms of horizontal
1421 displacement and rheology (strength profile), **(a)** at the onset of extension and **(b)** after a strong crustal
1422 thinning in the hyper-stretched portion of the lithosphere.

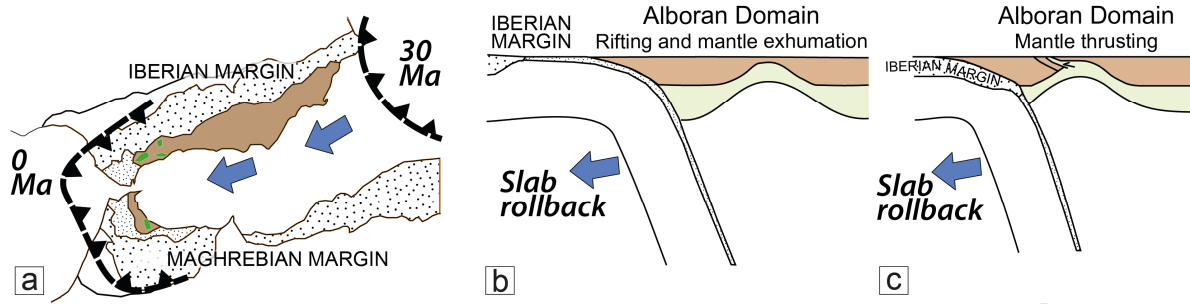
1423

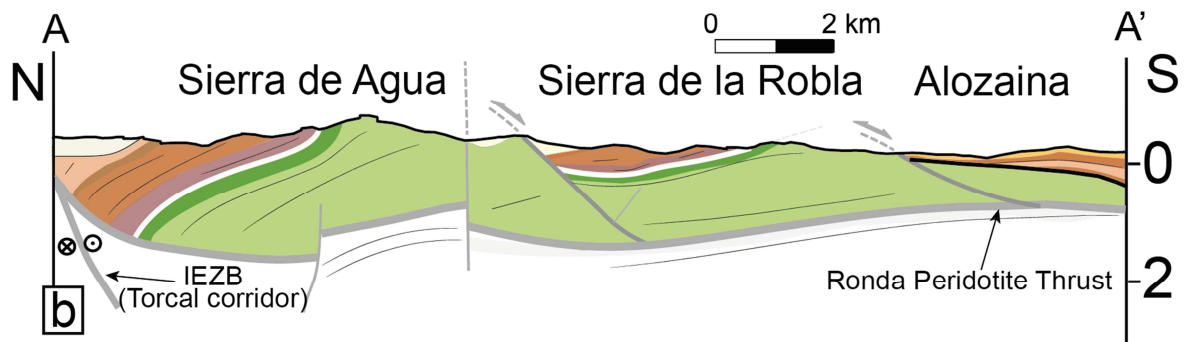
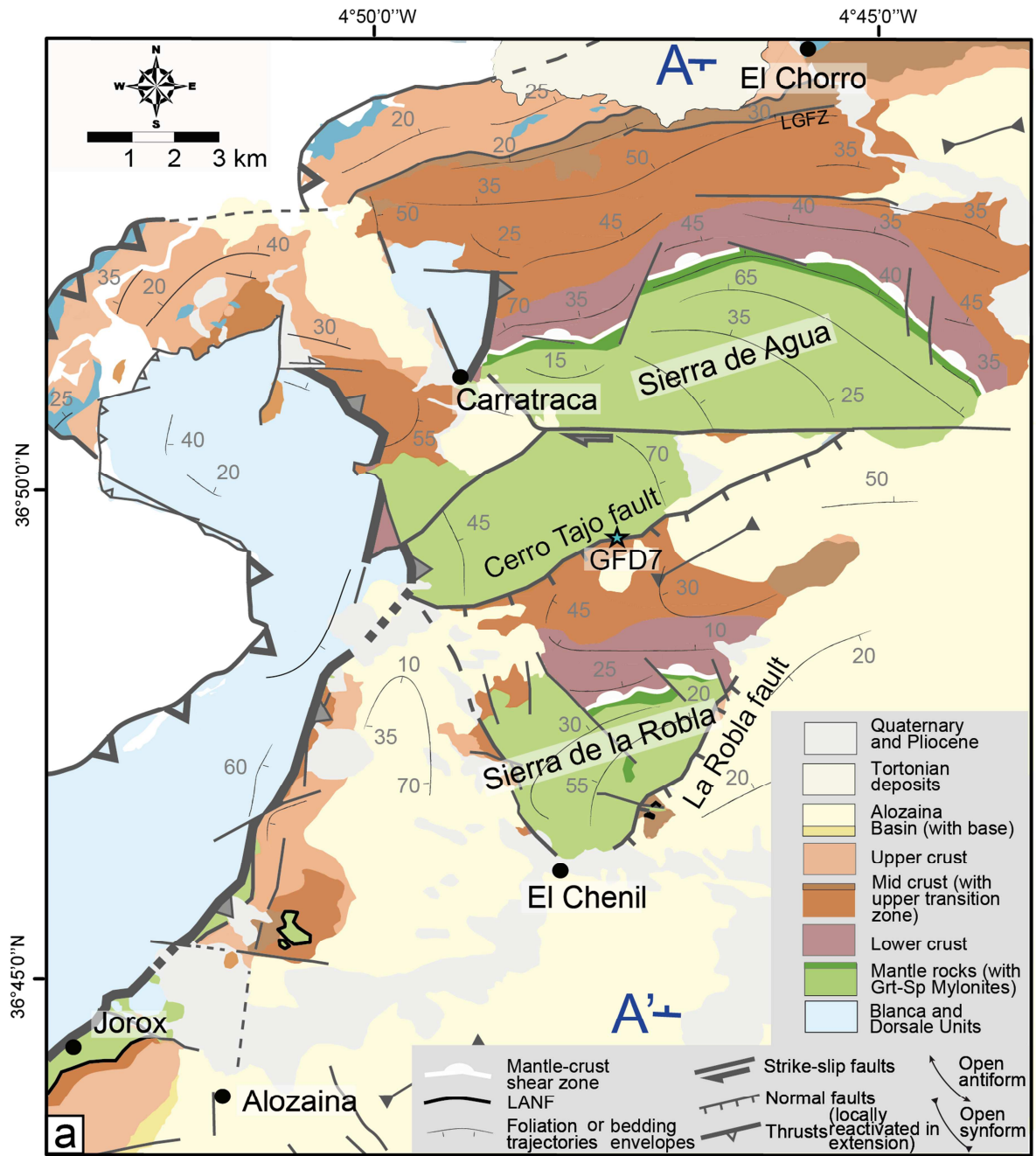
1424 **Fig. 10.** Three-stage conceptual model of lithosphere necking summarizing the progressive
1425 deformation recorded in the crust and mantle units of the Carratraca area. (a) Early stages controlled
1426 by the mid-crustal shear zone and the crust-mantle shear zone with opposite senses of shear. (b)
1427 Advanced stages characterized by localization of stretching at rift center leading to an extreme
1428 thinning of the ductile crust and omission of the lower crust. (c) Late stages of high-angle faulting
1429 cutting through the strongly attenuated crust and the cooling mantle.

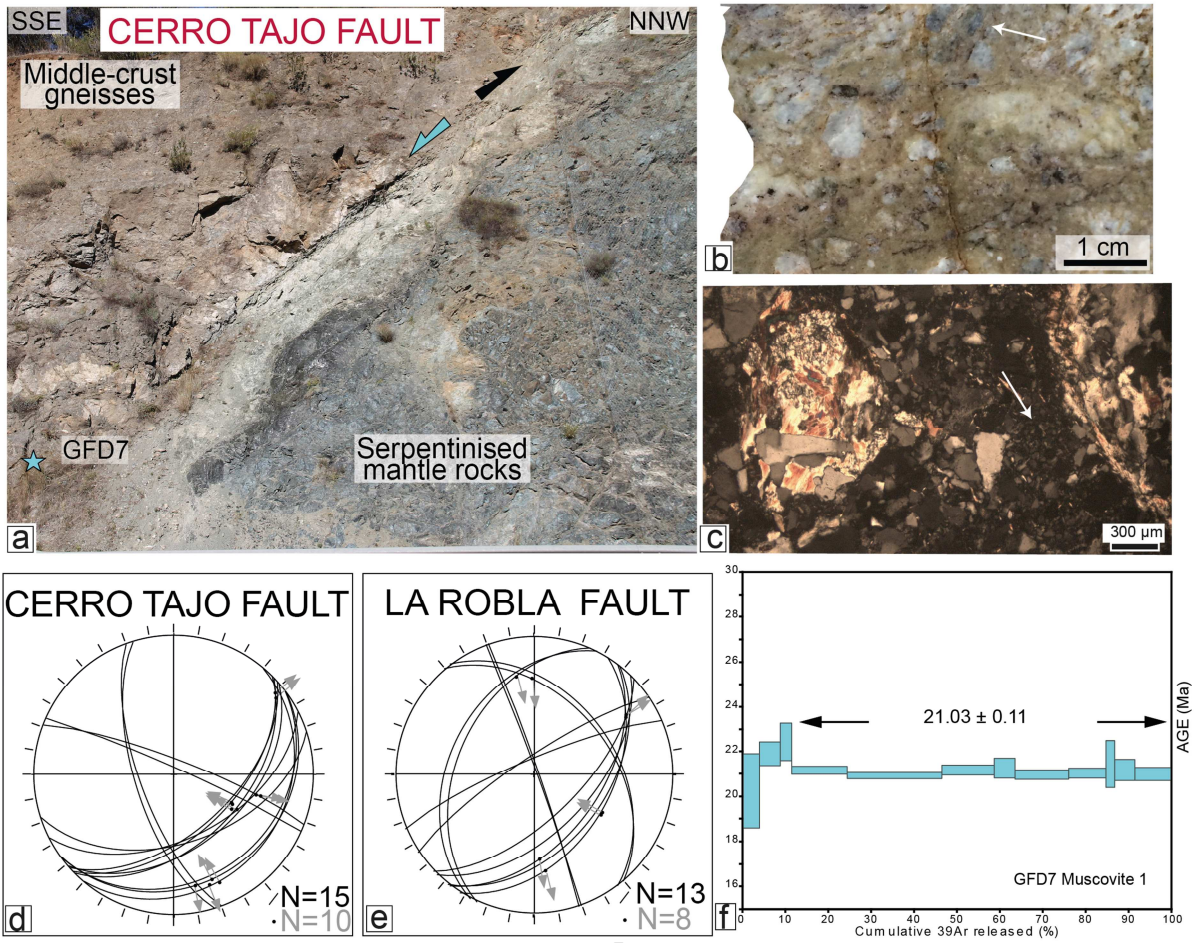
1430

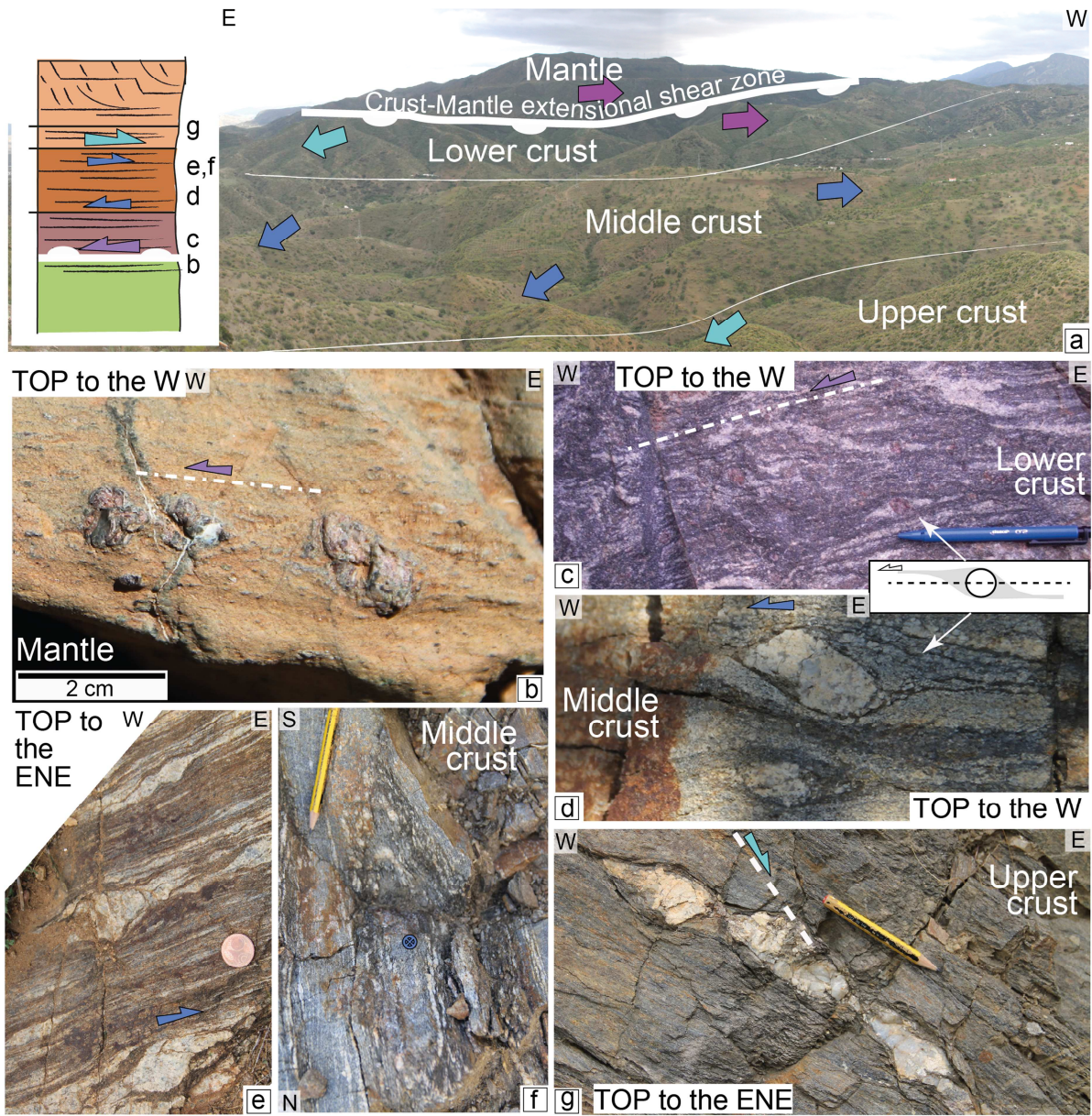
1431 **Fig. 11.** Comparison of models of lithosphere necking up to mantle exhumation, which evolve either
1432 dominantly symmetrical (a and b) or asymmetrical (c and d), with the lithosphere-scale deformation
1433 pattern documented in the western Betics (e and f) (as summarized in Figs. 9 and 10).

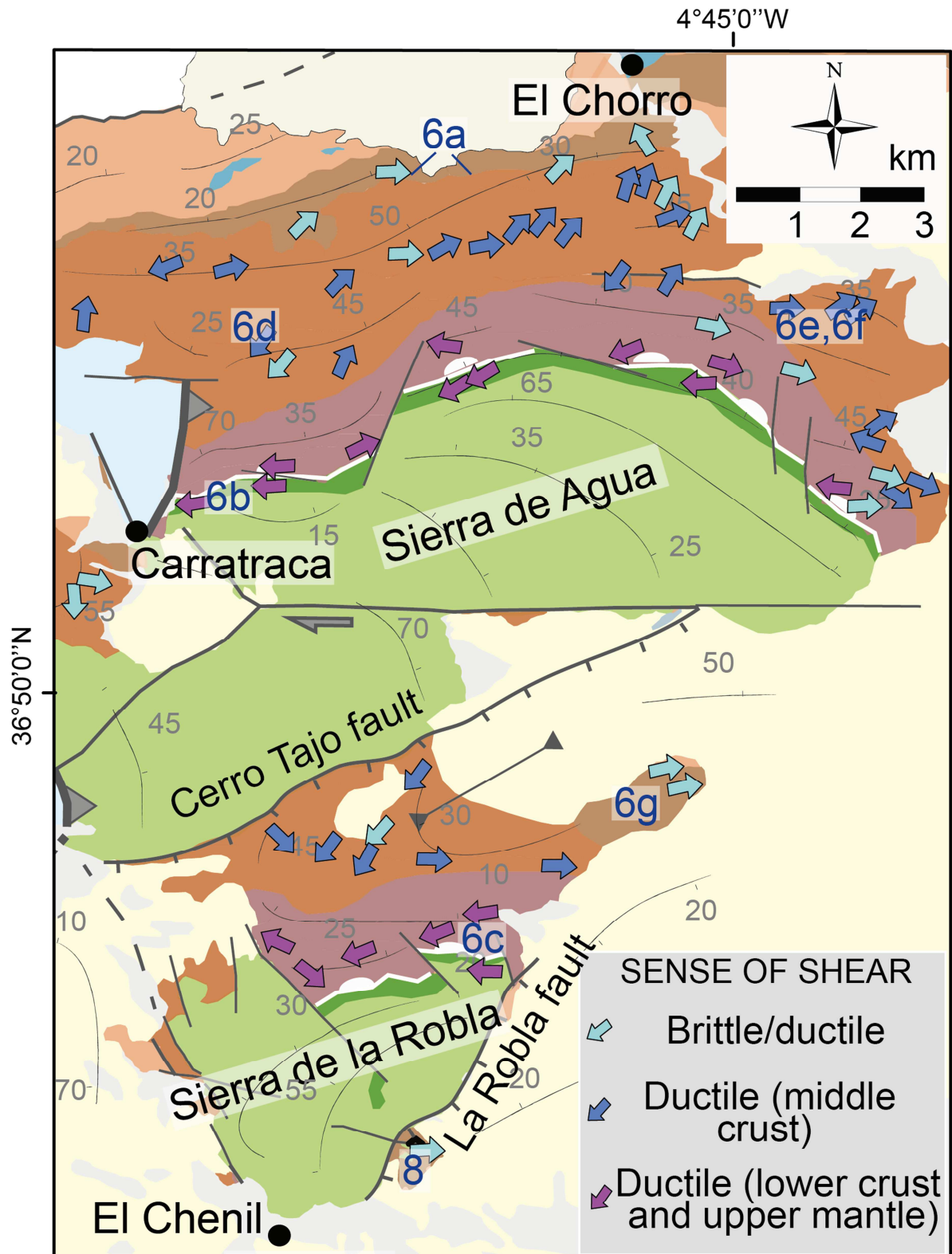


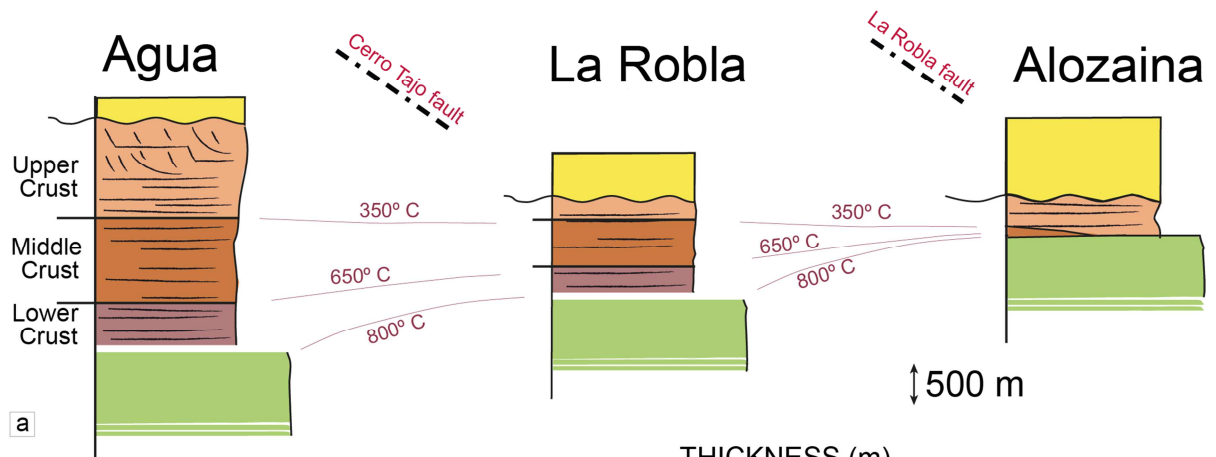










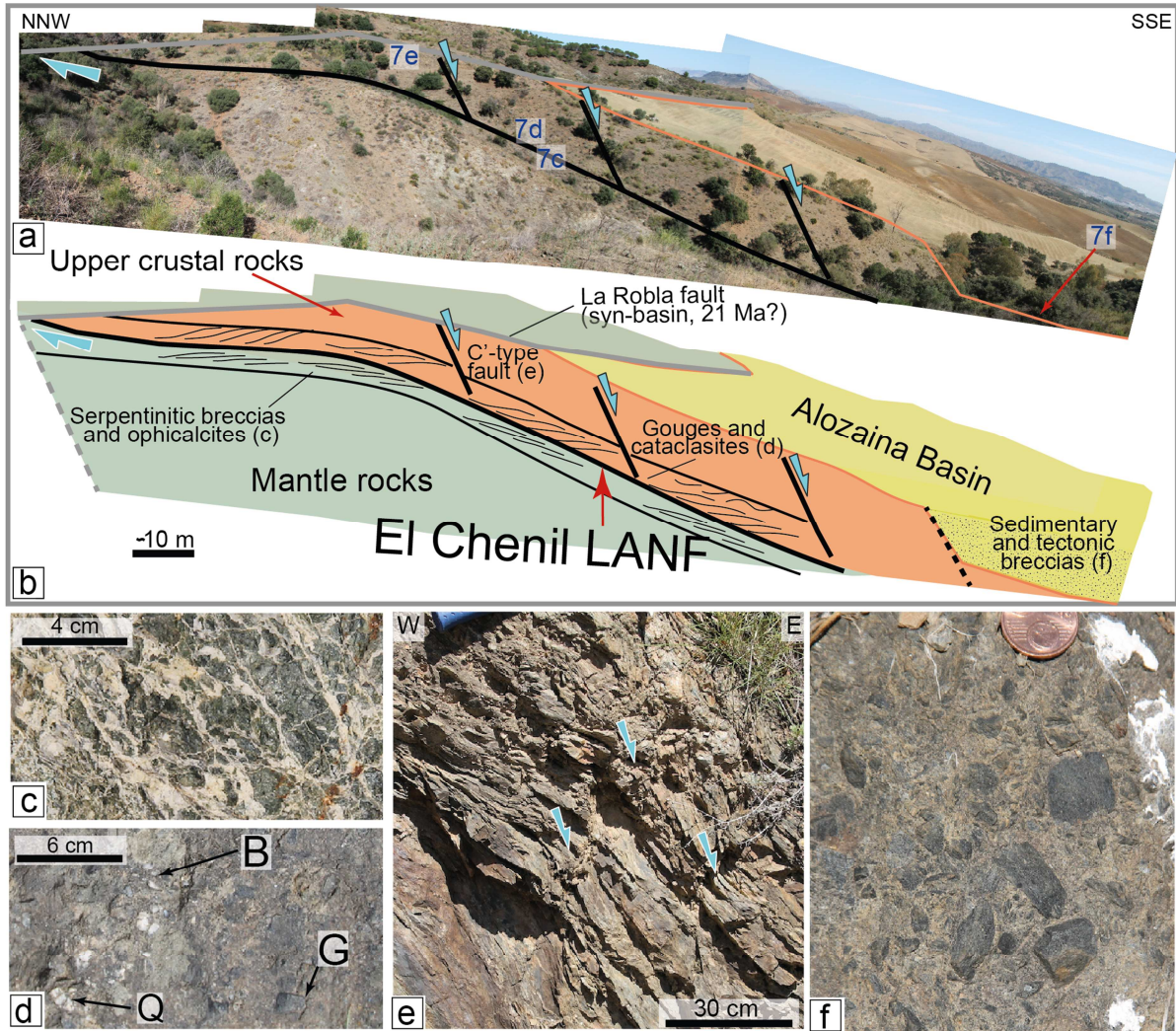


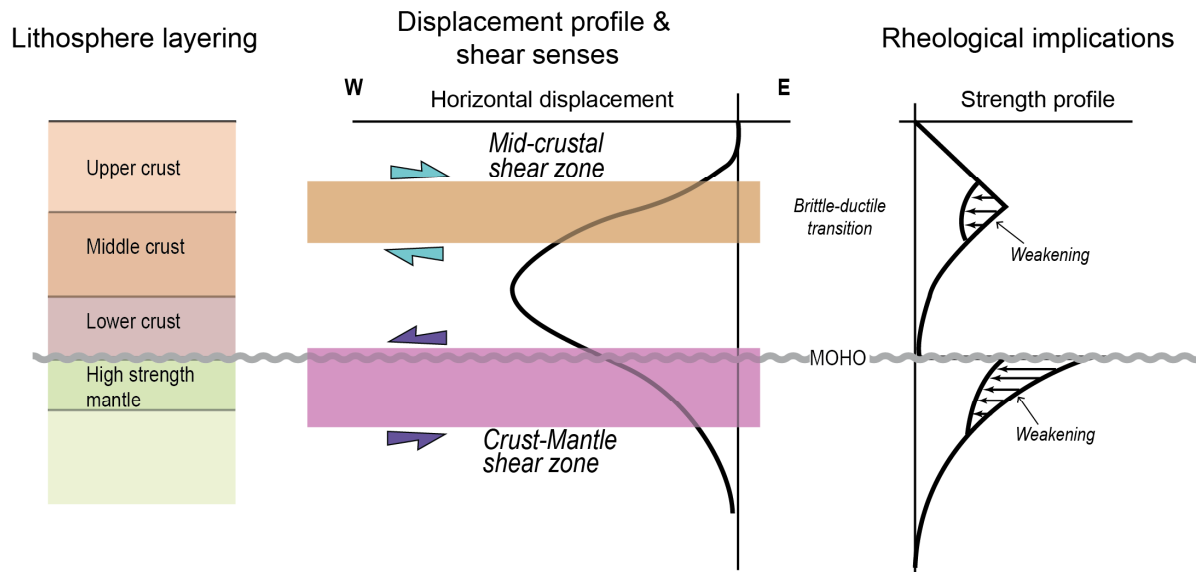
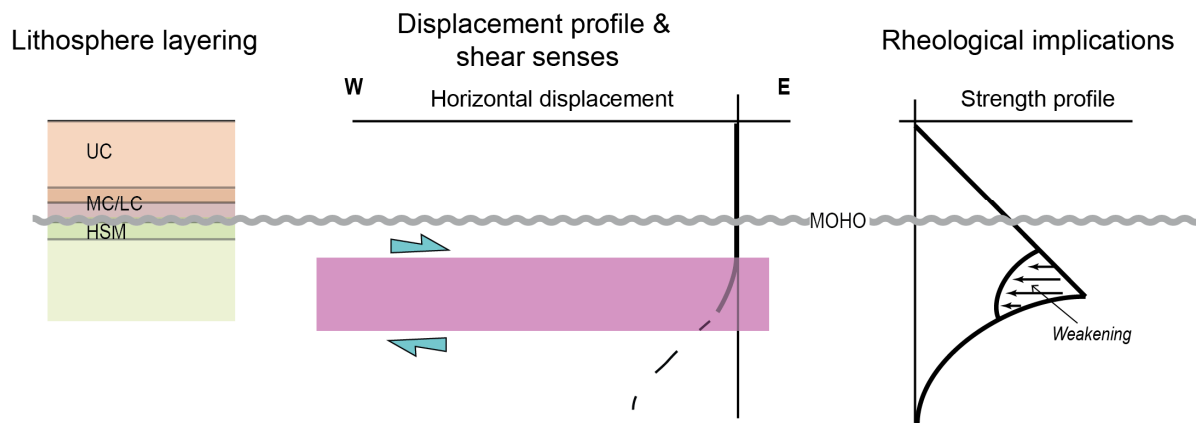
a

	THICKNESS (m)		
	Agua	Robla	Alozaina
Upper Crust totally or partly eroded	> 1270	0	> 480
Middle Crust	1510	950	50
Lower Crust	560	370	20
Ductile crust	1970	1070	70

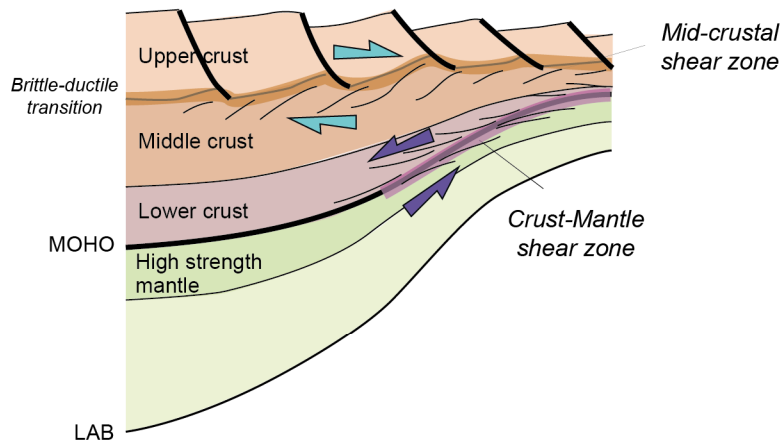
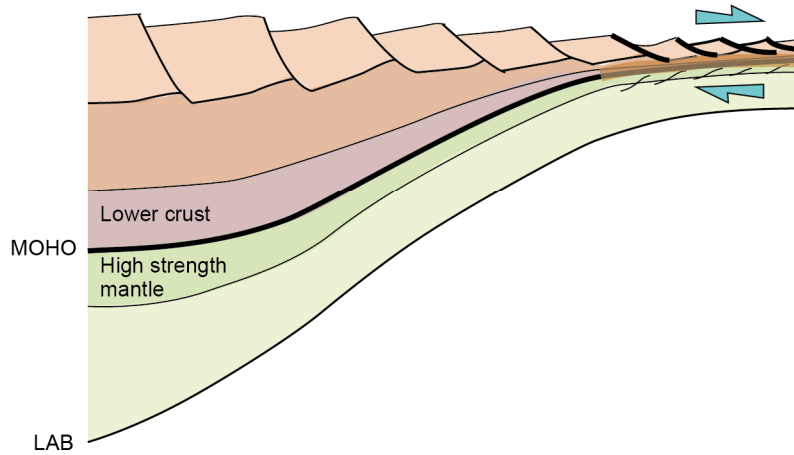
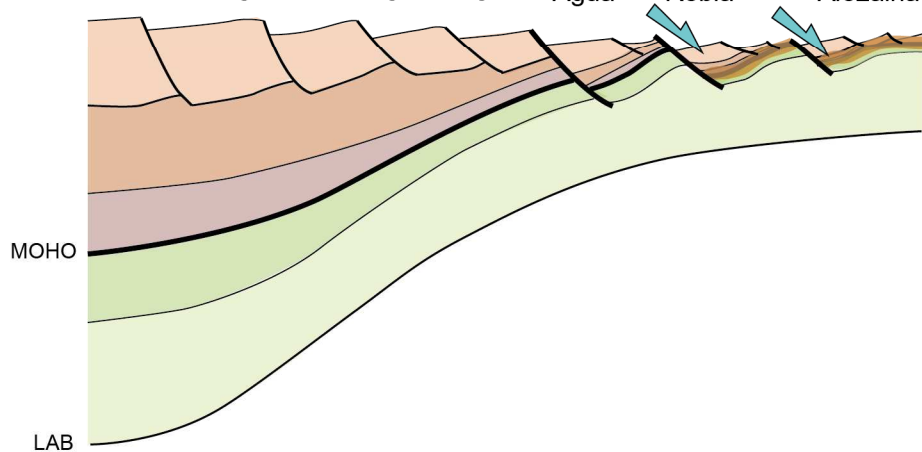
b

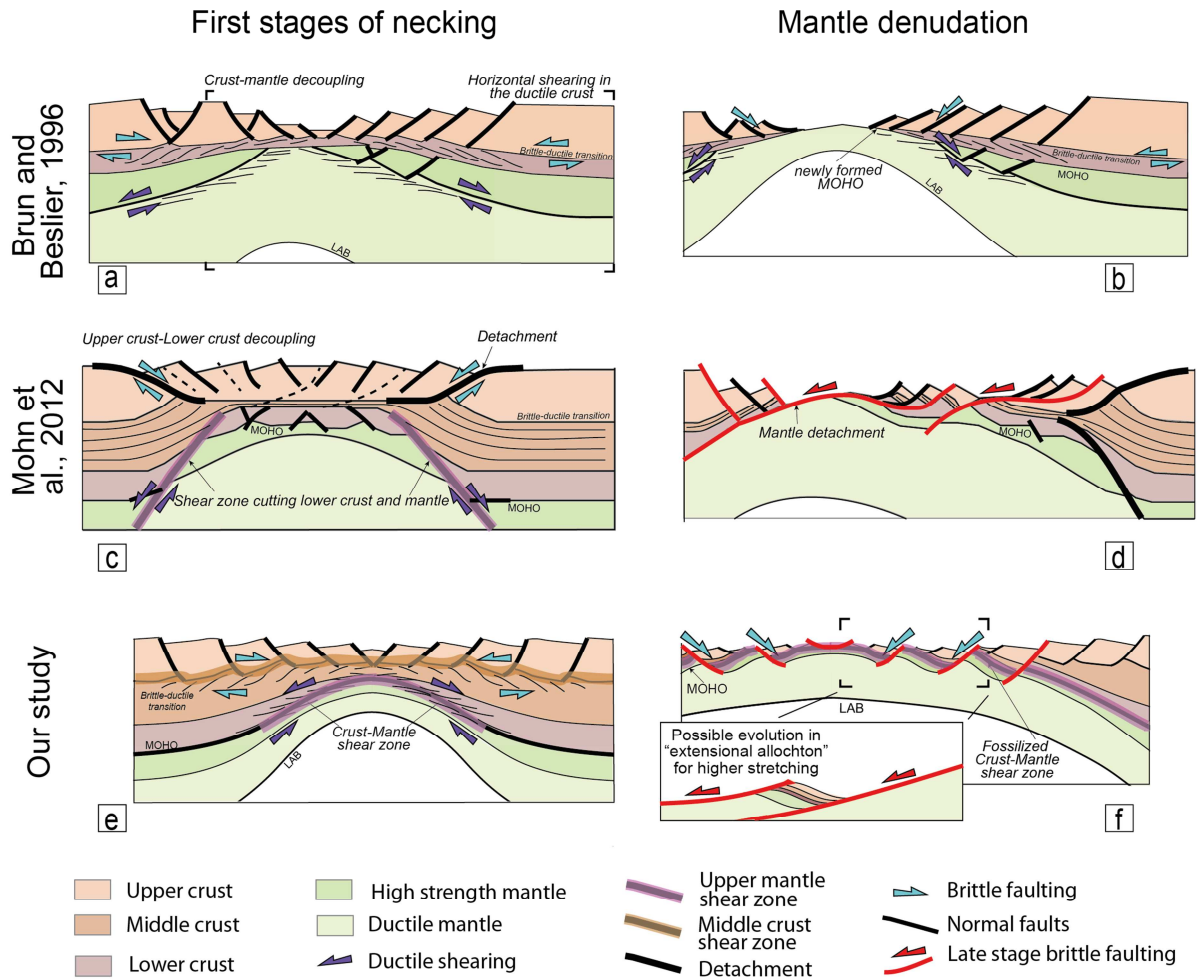
ACCEPTED MANUSCRIPT



a) At the onset of extension**b) After a significant amount of thinning (hyper-stretching)**

ACCEPTED

a 33-25 Ma; Early stages of lithosphere necking*Crust-mantle decoupling, crust heating by exhuming mantle***b** 25-22 Ma; Advanced stages of lithosphere necking*Crust-mantle coupling, localisation (hyper-stretching), onset of cooling***c** 22-20 Ma; Late stages of lithosphere necking*Mantle faulting & block tilting, cooling*



Highlights

- Western Betics (S Spain): exceptional exposures of thinned continental lithosphere
- Progressive lithosphere necking leads to crustal stretching values larger than 2000%
- 1) mid-crustal and crust-mantle shear zones act with opposite senses of shear;
- 2) ductile crust disappears, and upper crust touches the subcontinental mantle
- 3) high-angle normal faults end mantle exhumation where stretching is localized.